Università degli Studi del Piemonte Orientale

"Amedeo Avogadro"

Dipartimento di Scienze del Farmaco

Dottorato di Ricerca in Biotecnologie Farmaceutiche ed Alimentari

XXVI ciclo a.a. 2010-2013

NANOSYSTEMS FOR MOLECULAR IMAGING

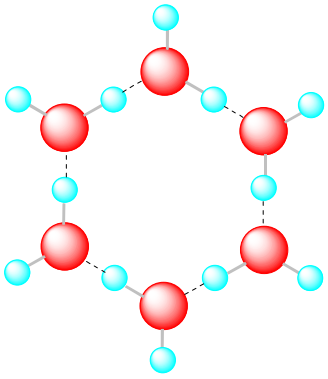

Valeria De Biasio

Università degli Studi del Piemonte Orientale

"Amedeo Avogadro"

Dipartimento di Scienze del Farmaco

Dottorato di Ricerca in Biotecnologie Farmaceutiche ed Alimentari

XXVI ciclo a.a. 2010-2013

NANOSYSTEMS FOR MOLECULAR IMAGING

Valeria De Biasio

Supervised by:

Prof. Giovanni B. Giovenzana

PhD program Coordinator Prof. Menico Rizzi

Contents

Introduction

Molecular Imaging

Molecular Imaging (MI) is a growing research discipline that can be defined as the *in vivo* characterization and measurement of biologic processes at the cellular and molecular level. Molecular approaches to diagnostics were developed few years ago and they have become available to detect diseases only recently. Molecular Imaging relies on molecular changes because they represent early indicators of pathologies before the latter reach a macroscopic level (Figure 1). In this emergent area of research it is mandatory to anticipate the time to detect molecular or cellular changes, into the body, to predict as soon as possible the disease (1, 2).

Molecular Imaging finds a huge variety of applications, not limited only to detection of a disease in a early stage. Angiogenesis, for example, is a normal process that develops naturally during embryonic development or the female reproductive cycle, etc.; nevertheless, the vascular growth can happen in an unrestrained way determining pathologic conditions. Loss of this regulation is known to occur in more than 30 different diseases, *e.g.*: cancer, cardiovascular and immunologic disease, diabetes, etc., and can be detected by MI. The latter can be used to locate apoptosis phenomena. Apoptosys is a physiologic process consisting in a programmed cell death. Perturbation of this equilibrium can be related to a huge variety of pathologies. Apoptosys reduction can be related to cancer, autoimmune diseases, and viral infections. An increase in apoptosys can be related to AIDS, neurodegenerative disorders, ischemia, stroke, myelodysplastic syndromes (3).

Several instrumental imaging techniques are used to detect molecular changes in living organisms tissues. The most common are:

i) Nuclear techniques, as Positron Emission Tomography (PET), Single Photon Emission Computed Tomography (SPECT),

ii) MR techniques, as Nuclear Magnetic Resonance Imaging (NMRI), Magnetic Resonance Tomography (MRT), Magnetic Resonance Spectroscopy

iii) Optical techniques, as Optical Tomography, Surface Weighted Imaging (reflectance diffuse tomography), Phase-array Detection, Confocal Imaging, Multiphoton Imaging, or Microscopic Imaging

iv) Acoustic techniques: Ultrasonography (US) and Photoacoustic Imaging

In addition to the above cited techniques, hyphenated ones are available where a suitable combination of two of them (*e.g.*: PET-MRI) allow to obtain images endowed with an higher degree of diagnostic information.

Figure 1

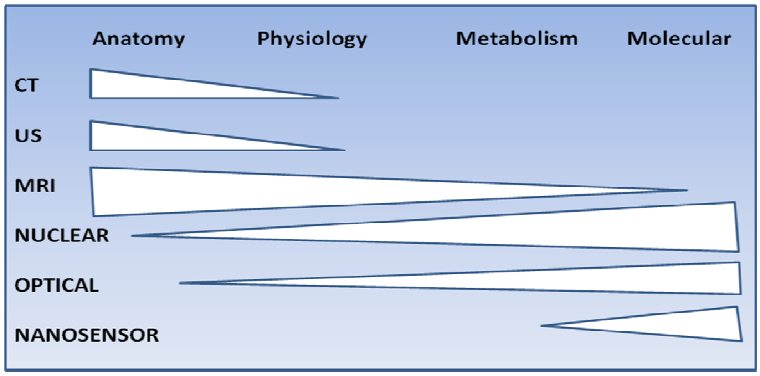

Figure 1 shows the different degree of diagnostic information associated with the single imaging technique, ultimately related to their resolution. For example X-Ray Computed Tomography, as Ultrasounds, allow to appreciate the anatomic structure of tissues while Magnetic Resonance Imaging, Nuclear Magnetic Resonance Imaging, Optical Imaging or Nanosensors, having a higher resolution, are able to give diagnostic informations ranging from physiological to the molecular level.

Molecular Imaging techniques

Optical Imaging

Optical Imaging encompasses several imaging modalities that can be applied to the diagnostic medical field to detect pathological changes in a non-invasive way, employing different kinds of "light" (UV, visible and IR). Processes can be investigated with Optical Imaging at several levels, at the organ, tissue, cellular and molecular one. The image, that derives from optical techniques, is produced by the interaction of different forms of light, depending on which technique is used. In particular, the image depends on the wavelength of the light that is used, from the instrument optical configuration employed to detect the signal and from auxiliary imaging agents used to give the contrast; the main limitation of OI is just related to the depth of penetration of light, ranging from < 1 mm for UV radiation to some centimeters for IR photons. When light interacts with tissues, the latter are involved in three processes: absorption, photon scattering and the generation of fluorescence emission (4). These three phenomena, on which is based Optical Imaging, are useful to recognize different tissues either functionally, for example to detect hemoglobin concentration, or structurally, *e.g.*: cellular morphology. The different Optical Imaging techniques are really a lot and generally they are based on the use of visible, ultraviolet and infrared light, absorbed, emitted or scattered by molecules of cells and tissues. Usually the techniques can be classified into Diffuse Optical Tomography (DOT) and Ballistic Optical Imaging (BOI), depending from principles are used to obtain the image (5). A special interest is hold by is Fluorescence Imaging. In this application, biocompatible fluorescent

dyes are used and if excitation in the IR region is adopted it is possible to perform *in vivo* imaging on whole small animals. A current limitation of this technique is the translation from animals to patients, as it means that for patients, for example, bulk tissues should not exceed in size over 10 cm (6). Optical imaging may be combined with different techniques to have more detailed images, as for example OI/MRI (7).

Exogenous imaging agents such as fluorescent dyes are used in Optical Imaging. Thousands of fluorescent dyes are known and some of them currently used in fluorescent imaging applications. Indocyanine green (ICG) is approved for *in vivo* use. Cyanines represent the largest family of fluorescent dyes and many hydrophilic or conjugated derivatives of cyanines have been synthesized to visualize *e.g.* tumor cells (8, 9). Rhodamine and fluorescein derivatives have been extensively employed and conjugated with small molecules acting as vectors to detect specifically tumor cells (10). Fluorescent sensors are also available for metal ions, changing their emission propertied in the presence of different concentrations of specific metal ions (for example Cu^{2+}) and being extremely useful for *in vivo* imaging applications. AlexaFluor® is another class of fluorescent dyes, widely used in virtue of the high intensity of fluorescence of these derivatives. Finally, the acronym BODIPY includes a class of fluorescent dyes where the core structure is represented by 4,4-difluoro-4-bora-3a,4a-diaza-s-indacene; this unusual heteropolycyclic structure is characterized by a very high quantum yield (11).

Positron Emission Tomography (PET)

PET is a diagnostic technique in which images are obtained using the positron emission of radionuclides, used in the form of radiolabeled agents. PET

radionuclides, emittes positrons that annihilates with nearby electrons, emitting two collinear opposite γ-rays. An array of detectors collect the radiation, discriminating the γ-rays pair emitted by the radionuclide on the base of their simultaneous detection an reconstructing the emission source point by retroprojecting their trajectories. Several positron emitting radionuclide are available, among them light atoms such carbon and fluorine and radiometals such as copper and gallium. Some of these elements are present into biomolecules into the body, and, this means that the use of positron emitting isotopes does not alter the physicochemical and biochemical properties with respect to the nonlabeled compounds (12). In PET applications, scientists prefer to use ^{18}F, in view of its availability, easy introduction in organic molecules and favourable emission energy. Its half-life, of 110 min, is compatible with 3-4 synthetic steps to be used to prepare labeled organic compounds. One of the most used PET agents is 2-[^{18}F]-fluoro-deoxy-D-glucose, also known like ^{18}F-FDG; it is used to monitor glucose metabolism and it is really important for clinical diagnosis of tumors, considering that tumoral cells are quite hungry of sugars. ^{11}C is another important positron-emitting isotope and it is less used to prepare organic compounds due to the short half-life of 20.3 min.

In addition to ^{11}C and ^{19}F, several metal isotopes find an application into PET-imaging, as ^{64}Cu, ^{76}Br, ^{68}Ga and that they are most of all used to study biochemical processes connected with slow pharmacokinetics (13).

PET imaging finds many diagnostic applications and it is best suited for detecting some kind of tumors, even if it is becoming a powerful tool in MI applications due to its relevant sensitivity. For example it is used to study the expression of somatostatin receptors, the latter being involved in: CNS, hypothalamopituitary system, gastrointestinal tract, exo- and endocrine pancreas, and immune system. It is used to explore the colinergic system, too,

because it can be involved in neurological and psychiatric disorders, as for example Alzheimer's and Parkinson's disease (14).

Single-Photon Emission Computed Tomography (SPECT)

Single-photon emission computed tomography (SPECT), together with PET imaging, was the first imaging modality used in clinical. For SPECT imaging, contrast agents are labelled with specific radionuclides, all able to emit γ rays. The energy arising in the form of radiation from these radionuclides, have to be in the range 100-250 keV to obtain good-quality images. The *γ*-rays used to create the images, are captured by detectors included into a so called "γ camera", and sent to an elaborator dedicated to the image reconstruction and editing. Many metal isotopes emit *γ*-rays useful for SPECT, as ^{67}Cu, ^{67}Ga, ^{111}In, ^{90}Y, ^{201}Tl, and their corresponding ions may be combined with suitable chelating agents to create γ-emitting complexes, to be conjugated with peptides, antibodies or other targeting vectors (15). Nevertheless, the most important element used for SPECT imaging is ^{99m}Tc, because when it emits γ rays, the energy released is of 140 keV (89% abundance), meaning that this element is perfect to be detected in imaging with a gamma camera. A drawback of using ^{99m}Tc is its relatively short half-life, about 6 h, hampering long and articulate preparations, but compensated by the availability of this nuclide through a dedicated generator. Nowadays applications with ^{99m}Tc can offer two possibilities to exploit this element, it means that it can be used to label a targeting moiety, as antibody, peptide, hormone, or using the ^{99m}Tc-chelate as such.

Radiopharmaceuticals containing ^{99m}Tc are used to study many diseases: ^{99m}Tc-diphosphonate radiopharmaceuticals are accumulated into bones, and this is important to detect bone metastases or hidden fractures. ^{99m}Tc-D,L-HM-PAO (Ceretec) and ^{99m}Tc-LL-ECD (Neurolite) for example allow to study blood flow into the brain, while ^{99m}Tc-sestamibi (Cardiolite) gives informations both for myocardial perfusion imaging and also for cancer imaging (16). Cu^{2+} has a rich coordination chemistry exploited to in a large variety of complexes with nitrogen-based ligands, including cyclen and cyclam derivatives. Considering that coordination numbers of this element range from 4 to 6, geometries of several Cu^{2+}-complexes can be square planar, square pyramidal, trigonal bipyramidal, and octahedral (17, 18). Several $^{67}Cu^{2+}$-complexes were studied for SPECT detection of tumors (19, 20). $^{67}Ga^{3+}$ recently received renewed interest for the preparation of chelates for SPECT due to the availability of this nuclide through a dedicated generator. Many derivatives have been reported in the scientific literature, mainly concentrated on hexacoordinated ligands that can match the coordination requirements of this “hard” trivalent ion (21).

SPECT was extensively employed in Molecular Imaging application, such as the sensitive detection of: folate receptors and oxytocin receptor that are generally over-expressed on tumoral cells, or integrins receptors, directly connected to inflammation, lung cancer, teratoma, etc. (22- 24).

X-Ray Computed Tomography (x-ray CT)

X-ray-computed tomography (CT) is a technique that allows to obtain three-dimensional images of tissues and screening diseases into a non invasively way. CT is a relatively old technique, having become a diagnostic tool when X-rays were discovered in 1895. Electromagnetic radiation of X-rays has wavelengths within the range of 0.01 and 10 nm. X-rays are generated in a vacuum tube where electrons are accelerated and travel from a catode to a tungsten-alloy anode; colliding with the anode electrons are braked, releasing X-rays with a specific energy dependent from the energy of incident electrons. CT is extremely versatile: gastrointestinal tract, cardiovascular system, renal tract, liver, lungs, bone, cartilage and some tumor tissues can be screened by this technique (25). Diagnostic images are formed by the absorption of X-rays from heavy atoms present in the tissue such as calcium. During CT contrast agents may be used; they generally contain atoms with an high atomic number, as I or Ba as the latter strongly absorb X-rays, and are employed to improve imaging of soft tissues.

Contrast agents based on iodine can be ionic or nonionic molecules usually belonging to the class of 2,4,6-triiodoarylcarboxamides. Ionic compounds are inclined to interact with biological molecules, as peptides or cell membranes, and may increase the plasma osmolality due to the large dose administered (26). For this reason generally nonionic contrast agents are preferred to the charged ones, even if nowadays both of them have been improved thanks to their manipulation, for example adding hydrophilic residues that allows higher solubility in water and lower toxicity (27). Among iodine contrast agents, the most used in CT are iopamidol, iomeprol, iohexol, iopromide. Barium sulfate, is a contrast medium widely used to image the gastrointestinal tract, as are other

triiodoaromatics (28, 29). A recently described Ca^{++}-based comtrast agent offers the possibility to study the biochemical state of a tissue, like for example bone or cartilage (30), exemplifying the use of X-ray CT in MI applications.

Ultrasounds echography (US)

Ultrasounds found a broad practical application in clinical diagnostics in virtue to their useful properties. Ultrasound echography is a relatively cheap technique giving the possibility to detect pathologies without relying on ionizing radiations like X-rays and γ-rays; in addition images are obtained in real time. This technique provides defined images of organs, for example hearth chambers and generally images of anatomical structures (e.g. fallopian tubes). Contrast agents, employed in this technique have to be able to reflect and scatter ultrasounds waves and to be necessary biocompatible.

Contrast agents used for ultrasounds are composed of microbubbles with a diameter in average of 1-7 μm. These can be used as tracers to study pathologies into the liver for example, like cirrhosis and metastases (31). The preparation of microbubbles generally is done into a biocompatible liquid, *e.g.:* saline or viscous dextrose or X-ray contrast solutions. The pulse of ultrasound excites the gas microbubble, and, in this way, thanks to the vibration of the bubble, secondary ultrasound waves are emitted with different intensities. Finally the reflectance of microbubbles provides a bright contrast. US images are exploited for echocardiography, Doppler macrovasculature, and Doppler microvasculature, depending on the area of interest and on the specific diagnostic need (32). The fluid employed to form microbubbles for US can be air, nitrogen, sulfur hexafluoride or perfluorocarbons such as perfluorooctane. Perfluorocarbons and SF_6 are chemically inert and can be efficiently closed

within microbubbles, and contribute to their stabilization. The first microbubble containing perfluorooctyl bromide ($C_8F_{17}Br$) conferred to emulsions a significant lipophilicity, so that it was used to study the gastrointestinal tract. SF_6 microbubbles, instead, are made of lyophilized phospholipids/polyethylene glycol/palmitic acid powder stored under SF_6 gas (33) and is used to detect liver lesions otherwise difficult to observe. Nevertheless, microbubbles result useful to detect many pathologies, as diseases of the heart, vascular structures, liver, breast, spleen, pancreas (cystic pancreatic masses with a different vascularization pattern) and gastrointestinal tract (Crohn's disease with a thickened bowel wall) (34-36). Targeted microbubbles are in development, in which specific molecules are included in the bubble external surface in order to direct them preferentially into tissues of interest, with a focused increase of the echogenic signal.

Magnetic Resonance Imaging (MRI)

Magnetic Resonance Imaging includes different techniques engaged to detect diseases at different levels: anatomical, physiological, metabolic and molecular. Thanks to the development of NMR techniques declined in clinical diagnostic modalities, a new class of pharmaceuticals, the MRI contrast agents (CAs) was developed. CAs are injected to a patient to enhance the image contrast between normal and diseased tissue and/or to indicate the status of organ function or blood flow. The image intensity in 'H NMR imaging, largely composed of the NMR signal of water protons, is dependent on nuclear relaxation times. Complexes of paramagnetic transition and lanthanide ions, which can decrease the relaxation times of nearby nuclei via dipolar interactions, have received the most attention as potential contrast agents.

^{1}H-NMR image intensity depends on relaxation times of protons in body tissues. In this technique, one or more radiofrequency pulses are used to perturbe the net macroscopic magnetization of proton spins, where the latter result aligned in a parallel way along the z axis with the applied field. The component of the magnetization, after being perturbed by the external field, from the z axis 'relaxes' back from its equilibrium value in an exponential way. This exponential time constant is called the longitudinal (or spin-lattice) relaxation time and it is indicated with T_1. Also the transverse magnetization decays coming back to its equilibrium value of zero, where the time dependence of the magnetization perpendicular to the z axis is called the transverse (or spin-spin) relaxation time, that is T_2. Generally, when acquiring NMR image data, many pulses are rapidly repeated and relaxation strongly affect the signal intensity due to its direct influence on magnetization recovery. Moreover, tissues with short T_1, give images with a greater intensity if they are compared to tissues with longer T_1 values, because the steady-state magnetization along the z axis is better recovered in the tissue with the fastest relaxation. Instead, if we consider T_2 constant, short values of this parameter are generally associated with a lower signal intensity, because the net transverse magnetization, that is important to detect the signal, is lower too (37, 38). The main purpose of NMR is to enhance the proton relaxation rate of water, ability known as relaxivity, to increase, finally, in a significant way, the relaxation rate of tissues of interest. This is possible using complexes with paramagnetic metals that exchange rapidly their coordinated water with the bulk water; the proton of coordinated water molecules relax very fast, and the fast exchange allows to spread the relaxation effect to the water molecules of the bulk solution. MRI CAs have to be non toxic, hence an outstanding thermodynamic and kinetic stability of the metal complexes is strictly required. The minimal dose, to produce relevant relaxation rates of tissues should increase $1/T_1$ enough for the tissue to be

detected by NMR imaging, and for the currently used Gd-complexes is about 0.1 mmol/Kg.

The diamagnetic and paramagnetic contributions to the relaxation rates of such solutions are additive and given by eq 1, where $(1/T_i)_{obsd}$ is the observed solvent relaxation rate in the presence of a paramagnetic species, $(1/T_i)_d$ is the (diamagnetic) solvent relaxation rate in the absence of a paramagnetic species, and $(1/T_i)_p$ represents the additional paramagnetic contribution.

$$(1/T_i)_{obsd} = (1/T_i)_d + (1/T_i)_p \qquad \boldsymbol{i} = 1, 2 \quad (1)$$

If there are no solute-solute interactions, relaxation rates of the solvent become linearly dependent on the concentration of the paramagnetic species ([M]); ***relaxivity,*** $\boldsymbol{r_i}$, is the slope of this dependence and it's expressed in units of $M^{-1}\ s^{-1}$ or, more commonly, $mM^{-1}\ s^{-1}$ (eq 2).

$$(1/T_i)_{obsd} = (1/T_i)_d + \boldsymbol{r_i}[M] \qquad \boldsymbol{i} = 1, 2 \qquad (2)$$

The magnetic field right around the paramagnetic center, given its large and fluctuating nature, gives an additional relaxation pathway for solvent nuclei.

Far from the paramagnetic center, these fields decrease suddenly, molecules of the solvent and of the complex start to have random translational diffusion and specific chemical interaction; this means that solvent molecules wander around the metal ion, arriving at a distance enough to transmit the paramagnetic effect (*e.g.*: within 5 Å).

The sum of these contributions gives the total relaxivity of the paramagnetic species. Relevant contributions to water proton relaxivity, may be ascribed to three types of interaction.

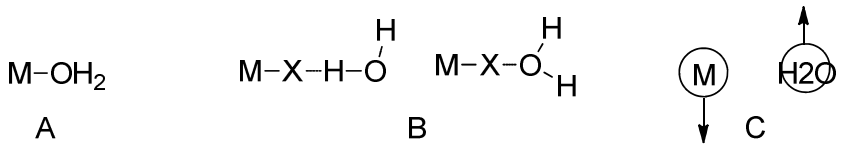

In the first mechanism (A) the interaction between the water molecule and the metal ion happens in its first coordination sphere, followed by the water molecule exchange with the bulk solvent. This is a relaxation mechanism that is called "inner-sphere relaxation". This behavior happens in the same way also for the case B, but the interaction, that is with hydrogen-bonded waters, involves the second coordination sphere. The mechanism of the second coordination sphere interactions is complex and not completely clarified; moreover it is not always possible to distinguish this relaxation mechanism (type B) from the type C, *i.e.*: translational diffusion of the water molecule around the chelate, referring simply to "outer-sphere relaxation". The total relaxivity of a paramagnetic agent is therefore generally given by eq 3.

$$(1/T_i)p = (1/T_i)_{\text{inner sphere}} + (1/T_i)_{\text{outer sphere}} \quad \boldsymbol{i} = 1, 2 \quad (3)$$

The inner sphere mechanism involves a chemical exchange of the water molecule between the primary coordination sphere of the paramagnetic metal ion and the bulk solvent and follows eq 4.

$$\left[\frac{1}{T_1}\right](\text{inner sphere}) = \frac{P_M q}{T_{1M}+\tau_M} \qquad (4)$$

P_M is the mole fraction of metal ion, q is the number of water molecules bound per metal ion, T_{1M} is the relaxation time of the bound water protons, and τ_M is the residence lifetime of the bound water.

The correlation times τ_C and τ_E, as given by eq 6 and 7, regulate the dipolar and scalar relaxation mechanisms.

$$\frac{1}{\tau_C} = \frac{1}{T_{1e}} + \frac{1}{\tau_M} + \frac{1}{\tau_R} \qquad (5)$$

$$\frac{1}{\tau_e} = \frac{1}{T_{1e}} + \frac{1}{\tau_M} \qquad (6)$$

T_{1e}, is the longitudinal electron spin relaxation time, τ_M is the water residence time and τ_R is the rotational correlation time of the entire paramagnetic (metal-water) assembly. The rotational correlation time is a parameter whose variation lead to remarkable effect on the relaxivity; for this reason the research of this PhD has been focused on nanosystems, where the increase in the size of the paramagnetic system is immediately reflected in the reduction of its tumbling rate, with significant increase of τ_R (39).

Nanostructures for Diagnostic Applications

Nanostructures, are systems composed of atoms or molecules of few units till to thousands ones with dimensions of the order of nanometers. Depending on dimensions, nanostructures can be classified in different classes: nanofabrics where the range of the height varies from 0.1 to 100 nm while the depth and width are bigger than nanometer dimensions; nanotubes, like carbon nanotubes, present a nanometric diameter and nanoparticles that have all three dimensions, height, depth and width, of the order of nanometers. To understand the order of magnitude of such particles, it should be noted that the wavelength of photons in the visible spectrum, is much longer than the diameter of the largest nanoparticle. Special instruments can be used to study nanoparticles, such as electron microscopes, or soft and hard X-rays, the use of which, however, is much more complex.

The study of nanosized systems began in the eighties to understand the behavior of matter at the mesoscopic level as it is an important link between the macroscopic matter, whose properties are described by thermodynamics and statistical mechanics, and the microscopic matter (the single atom or molecule). This is important because nanosized systems have some properties that are not showed in macroscopic systems, like transition from van der Waals bonding to metallic bonding in clusters of mercury; transition from paramagnetic to ferromagnetic behavior that has totally disregarded the prior knowledge on the magnetic properties of certain materials; interface between liquid and nanosized solid that presents many interesting aspects about the melting points and the nature of metastable phases, stages and sub-cooled overheated.

Commonly defined nanoparticle vectors include: liposomes, micelles, dendrimers, solid lipid nanoparticles, metallic nanoparticles, semiconductor

nanoparticles and polymeric nanoparticles, although the scope of nanoparticle formulations that have been applied to cancer therapy is far more elaborate (40, 41).

Depending on the chemical composition of the nanoparticles, they can carry a wide variety of compounds, making them efficient drug delivery vehicles. Polymers, dendrimers and lipidic nanosystems represent three-dimensional networks that form the matrix system and this one is used to encapsulate active principles. Several kinds of drug vectors have been investigating to increase specificity and activity for drug delivery systems and at the same time to reduce toxicity ensuring maximum treatment safety.

Many active pharmaceuticals ingredients (APIs) are not capable to cross the biological barriers that separate the administration site from the site of action due to physicochemical characteristics, while their inclusion in a nanosized system may represent an alternative pathway to enter the target site.

Sometimes APIs collide with enzymatic barriers, which lead to their degradation and fast metabolization. Therefore these active molecules can difficulty distribute themselves into the diseased target zones and may accumulate themselves in healthy tissues leading to unwanted toxic effects. Inclusion in a nanosized system may efficiently shield the API from the degradative activities of metabolic enzymes.

In addition, installation on the surface of the nanosystem of highly specific vectors lead to the delivery of the API to to the desired action site. Carriers of this type for drug delivery were created in the last twenty years and new medicines are developed to be delivered by matrix or vesicular carriers, such as doxil, where the drug is inside the liposomes is used for cancer treatment, or dendridic vectors used for transfection (42).

Figure 2

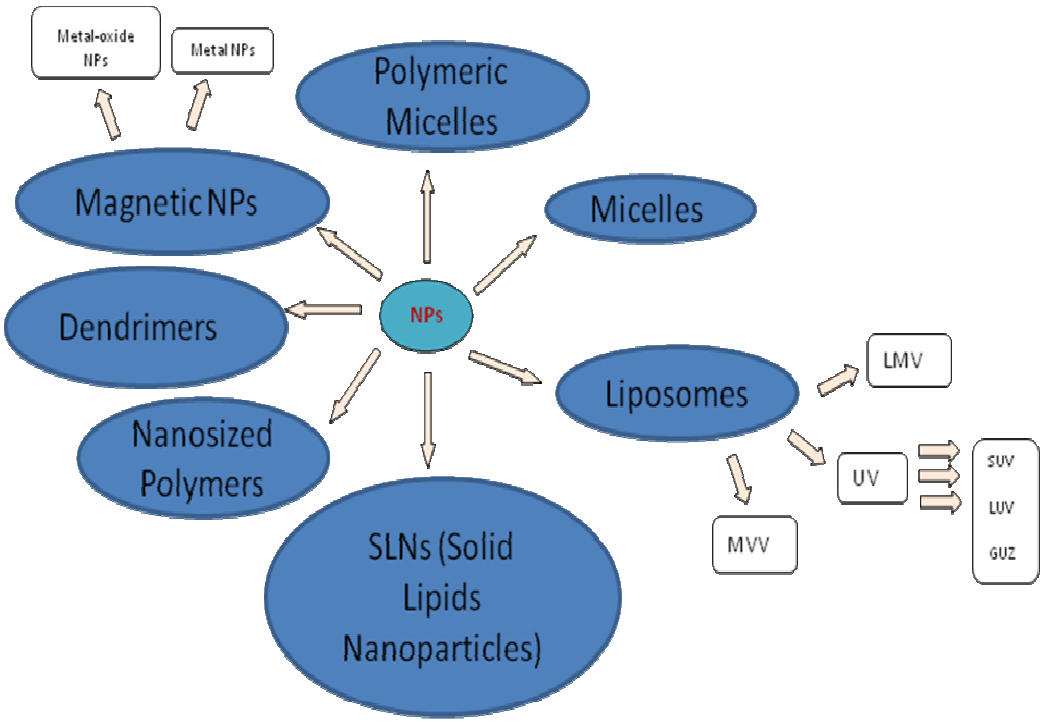

Figure 2: *Nanosized systems employed in Molecular Imaging.*

Micelles are aggregates of amphiphilic molecules in which the polar head groups are in contact with water while the hydrophobic moieties are located in the particle core to minimize their contact with water. In non-polar solvent the orientation is reversed and the micelle is called "reverse micelle". Micelles can assemble in different shapes, such as spherical, cylindrical, lamellar and disk-shaped. Micelles can form above the critical micelle concentration (CMC) and the size can vary from 1 nm to 100 nm. This system should be thought like a

dynamic structure because there is a continuous exchange between micelles and the aqueous solution.

Generally it is possible to modify the surface of the original mixture of micelle-forming surfactants adding new co-surfactants and also size and charge of these systems according always to the molecule that has to be transported (43).

It is really common to use PEG surface modification to avoid uptake by the reticuloendothelial system and mononuclear phagocytes, obtaining in this way stealth-shielded nanoparticles (44). There are also polymeric micelles that are generally more stable than surfactant micelles, and form at markedly lower CMCs. These are less dynamic than those formed from surfactants and it has been demonstrated that if free polymers are separated from polymers forming micelles they are still stable even if CMC decreases (45).

One or several phospholipid bilayers can auto-associate among themselves to form liposomes, leaving an aqueous compartment inside the structure. This structure is strongly similar to cell membranes and has been the subject of study of many research groups in chemistry, biophysics and pharmaceutics.

Liposomes for their composition and also for the preparation method can present different features. Liposomes are usually prepared in simple multi-step operations:

- dissolution of the lipids in an organic solvent
- solvent evaporation
- dispersion of the dried lipids in an aqueous solution

The main differences can arise on the method used to disperse the dried lipids: lipid dispersion can be obtained by hydration of the phospholipid film, sonication, microfluidification, extrusion, reverse-phase evaporation, ether infusion, injection of an ethanol solution, freeze-drying/rehydration, freezing/thawing, surfactant removal, or electroformation. The liposome

characteristics depend on the preparation technique and in this way the main size of these supramolecular structures can be from tens to a hundred micrometers. The number of lipidic bilayers can vary so that liposomes can be classified into: MLV (Multilamellar Vesicles) present a diameter more than 0.5 μm, UV (Unilamellar Vesicles) with a diameter more than 1 μm and MVV (Multi Vesicular Vesicles) with a diameter more than 1 μm and many vesicles inside the liposome. Unilamellar vesicles can be divided into three subclasses: SUV (Small Unilamellar Vesicles), with a diameter between 20 and 100 nm, LUV (Large Unilamellar Vesicles), with diameters above 100 nm, GUV (Giant Unilamellar Vesicles), with diameters above 1 mm (46).

These lipidic supramolecular systems are endowed with several advantages, and have been used as a vector for drugs. Moreover they are able to include both hydrophobic compounds, anchored into the bilayer, or hydrophilic substances, encapsulated in their cavity.

The passive encapsulation technique consists to rehydrate the lipidic film in the presence of the active substance (47), while the active process is applied after having made liposome using a concentration or pH gradient and it consists to mix hydrophobic drugs with phospholipids before the formation of the lipidic film (48, 49).

Solid lipid nanoparticles (SLN) are made generally of glycerides and present a diameter that can vary from 50 to 1000 nm. These nanoparticles can be obtained by different methods as high pressure homogenization, microemulsion, nanoprecipitation, where crystallinity of lipids can be different and the degree of this depends on the method which is used to product SLNs. The technique chosen to prepare SLNs is important because crystalline polymorphism defines the colloidal stability of these systems (50).

Nanoparticles can be constituted by metals or metal oxides for use as MRI contrast agents. For example there are two types of iron oxide mainly

investigated for their properties of superparamagnetism as maghemite (γ-Fe_2O_3) and magnetite (Fe_3O_4). Superparamagnetism is a really important property that allows for stability and individual dispersion of the particles after that an external magnetic field has been removed (51). Another class of metal nanoparticles are gold-nanoshells where there is an external Au-coating around a silica core, giving them a favourable use as contrast agents in optical coherence tomography, because variations in their size and shape allows for the precise tuning of their resonance wavelength (52).

Dendrimers are molecules composed of monomers with a central plurifunctional core and a tree-like growth process around. Due to their large number of surface groups and monodispersity, dendrimers have the ability to create multivalent interactions leading to their efficient use as vectors (53).

Polymers are large molecules composed of many repeated subunits. Polymers, both natural and synthetic, are created via polymerization of many monomers and so their consequently large molecular mass relative to small molecule compounds produces unique physical properties. Moreover incorporating inorganic nanostructures into a polymer matrix, the properties of both materials can be synergistically combined to create new attributes.

Metal-organic frameworks (MOFs) are also known as coordination polymers and they consist into an hybrid system made of metal connecting points and organic bridging ligands (54, 55). In the structure of MOFs bridging ligands can connect either metal ions or small metal clusters. These systems show really interesting properties, mainly due to their wide porosity with tunable pore sizes, shapes and functionalities. High agent loadings through several methods (direct incorporation into the framework or post-synthetic modification), intrinsic biodegradability from labile metal-ligand bonds, high porosity for loading/release of entrapped agents, and versatile functionalization methodologies, making them suitable to be used in biological research.

References

1 Weissleder R and Mahmood U (2000), *Radiology*, **219**, 316-333

2 Weissleder R (2006), *Science*, **312**, 1168-1171

3 Harisinghani MG, Barentsz J, Hahn PF, Deserno WM, Tabatabaei S, van de Kaa CH, de la Rosette J, Weissleder R. (2003), *N. Engl. J. Med.*, **348**, 2491-2499

4 Hawrysz D J, Sevick-Muraca E M (2000), *Neoplasia*, **2**, 388–417

5 Weissleder R, Ntziachristos V (2003), *Nat. Med.*, **9**, 123–128

6 Cutler M, (1929), *Surg. Gynecol. Obstet.*, **48**, 721– 729

7 Schoder H, Erdi Y E, Larson S M, Yeung H W (2003), *Eur. J. Nucl. Med. Mol. Imaging*, **30**, 1419– 1437

8 Haglund M M, Hochman D W, Spence A M, Berger M S (1994), *Neurosurgery*, **35**, 930–940

9 Ntziachristos V, Yodh A G, Schnall M, Chance B (2000), *Proc. Natl. Acad. Sci. U. S. A.*, **97**, 2767– 2772

10 Guo Z, Park S, Yoon J, Shin I (2014), *Chem. Soc. Rev.*, **43**, 16.

11 Nakayama A, Del Monte F, Hajjar R J, Frangioni J V (2002), *Mol. Imaging*, **1**, 365-377

12 Levin C S, (2005), *Eur. J. Nucl. Med. Mol. Imaging*, **32**, 325-345

13 Becherer A, Szabó M, Karanikas G, Wunderbaldinger P, Angelberger P, Raderer M, Kurtaran A, Dudczak R, Kletter K (2004), *J. Nucl. Med.*, **45**, 1161-1167

14 Reivick M, Kuhl D, Wolf A, Greenberg J, Phelps M, Ido T, Casella V, Hoffmann E, Alavi A, Sokoloff L (1979), *Circ. Res.*, **44**, 127-137

15 Welch M J, Redvanly C S, Eds, *Handbook of Radiopharmaceuticals: Radiochemistry and Applications*; John Wiley & Sons Inc.: Hoboken, NJ, 2003

16 Meares C F, Chen X, Ed (2009), *Recent Advances of Bioconjugation Chemistry in Molecular Imaging*, 227-241.

17 Kaden T A, Gokel G W, Ed (1993), *Advances in Supramolecular Chemistry* Elsevier, **3**, 65

18 Suchy M, Hudson R H (2008), E. *Eur. J. Org. Chem.*, **29**, 4847-4865

19 Fomenko V V, Polynova T N, Porai-Koshits M A, Varlamova G L, Pechurova N I (1973), *Zh. Strukt. Khim.*, **14** (3), 571

20 Broan C J, Cox J P L, Craig A S, Kataky R, Parker D, Harrison A, Randall A, Ferguson G (1991), *J. Chem. Soc., Perkin Trans.*, **2** (1), 87-91

21 Henze M, Schuhmacher J, Hipp P, Kowalski J, Becker D W, Doll J, Macke H R, Hofmann M, Debus J, Haberkorn U (2001), *J. Nucl. Med.*, **42** (7), 1053-1056

22 Sharma V, Beatty A, Wey S P, Dahlheimer J, Pica C M, Crankshaw C L, Bass L, Green M A, Welch M J, Piwnica-Worms D (2000), *Chem. Biol.*, **7** (5), 335-343

23 Sharma V, Prior J L, Belinsky M G, Kruh G D, Piwnica-Worms D (2005), *J. Nucl. Med.*, **46** (2), 354-364

24 Sharma V (2004), *Bioconjugate Chem.*, **15** (6), 1464-1474

25 Smith-Bindman R, Lipson J, Marcus R, Kim K-P, Mahesh M, Gould R, Berrington de Gonzalez A, Miglioretti D L (2009), *Arch. Intern. Med.*, **169**, 2078-2086

26 Christiansen C (2005), *Toxicology*, **209**, 185-187

27 Anelli P, Brocchetta M, Fretta R, Lattuada L, Mortillaro A, *WO2010105983* (**A1**), 2010

28 Garrett P R, Meshkov S L, Perlmutter G S (1984), *Radiology*, **153**, 545-546

29 Raptopoulos (1989), *V. Radiol. Clin. N. Am.*, **27**, 631-651

30 Goldring S R J (2009), *Bone Joint Surg.-Am.*, **91A**, 4

31 Schutt E, Klein D, Mattrey R, Riess J (2003), *Angew Chem Int Ed Engl*, **42**, 3218-3235

32 Blomley M, Cosgrove D, Albrecht T (1998), *Radiology*, **224**, 124-134

33 Schneider M (1999), *Echocardiography* **16** (7, Pt 2), 743–746

34 Nanda N C, Wistran D C, Karlsberg R P, Hack T C, Smith W B, Foley D A, Picard M H, Cotter B (2002), *Echocardiography*, **19**(1), 27–36

35 Sidhu P S, Allan P L, Cattin F, Cosgrove D O, Davies A H, Do D D, Karakagil S, Langholz J, Legemate D A, Martegani A, Llull J B, Pezzoli C, Spinazzi A (2006), *Br J Radiol*, **79** (937), 44–51

36 De Pascale A, Garofalo G, Perna M, Priola S, Fava C (2006), *Radiol Med*, **111**, 539–550

37 Farrar T C, Becker E D*, Pulse and Fourier Transform NMR*, Academic Press: New York, 1971

38 Greif WL, Buxton RB, Lauffer RB, Saini S, Stark DD, Wedeen VJ, Rosen BR, Brady TJ (1985), *Radiology*, **157**, 461-466

39 Solomon I (1955), *Phys. Rev.*, **99**, 559

40 Fonseca C, Simoes S, Gaspar R (2002), *J. Control. Release*, **83** (2), 273-286

41 Uhrich K E, Cannizzaro S M, Langer R S, Shakesheff K M (1999), *Chem. Rev.*, **99**, 3181-3198

42 Mall S, Buckton G, Rawlins D A (1996), *J. Pharm. Sci.*, **85**, 75-78

43 Kataoka K (1994), *J. Macromol. Sci. Pure Appl. Chem.*, **31**, 1759-1769

44 Brannon-Peppas L, Blanchette J O (2004), *Adv. Drug Del. Rev.*, **56**, 1649-1659

45 Malmsten M, *Surfactants and Polymers in Drug Delivery,* Marcel Dekker, New York, 2002

46 Colletier J P, Chaize B, Winterhalter M, Fournier D (2002), *BMC Biotechnol.*, **2**, 9-15

47 Abraham S A, McKenzie C, Masin D, Ng R, Harasym T O, Mayer L D, Bally M B (2004), *Clin. Cancer Res.*, **10**, 728-738

48 Stevens P J, Lee R J (2003), *Anticancer Res.,* **23**, 439-442

49 Müller R H, Mäder K, Gohla S (2000), *Eur. J. Pharm. Biopharm.*, **50**, 161-178

50 Gupta A K, Gupta M (2005), *Biomaterials*, **26**, 3995-4021

51 Chen J, Saeki F, Wiley B J, Cang H, Cobb M J, Li Z Y, Au L, Zhang H, Kimmey M B, Li X, Xia Y (2005), *Nano Lett.*, **5** (3), 473-477

52 Bromberg L E, Ron E (1998), *Adv. Drug Delivery Rev.*, **31**, 197-221

53 Bradshaw D, Warren J E, Rosseinsky M J (2007), *Science*, **315**, 977–980

54 Yaghi O M, O'Keeffe M, Ockwig N W, Chae H K, Eddaodi M, Kim J (2003), *Nature*, **423**, 705–714

55 Kayser O, Lemke A, Hernandez-Trejo N, (2005) *Curr Pharm Biotechnol* **6**, 3-5.

Outline of the thesis

The PhD research activity was devoted to explore original nanosystems for Molecular Imaging diagnostic applications. In this wide area of research, the activity of all three years was focused on the design, the preparation and the testing of novel and improved components for nanosized CAs for MRI.

The choice of MRI resides in its enormous potential in Molecular Imaging applications, where the superior resolution attainable led to extensive use of this diagnostic technique. The research group in which this PhD work was carried out has nearly 20 years of experience in MRI CAs, and the collaborations established in this period allow to perform a comprehensive and detailed evaluation of the compounds synthesized.

While resolution of MRI images is already very high, its sensitivity is far from optimal, suffering from the need for a significant concentration of paramagnetic species in order to obtain a suitable contrast efficiency. At least 10^7-10^8 molecules are needed to clearly visualize one cell, compared to the 10^2-10^3 molecules/cell required for Optical Imaging and the 10^0-10^1 molecules/cell needed for visualization with PET/SPECT techniques.

Nanosized systems are especially suited to solve the sensitivity problems, as a single nanometric assembly used as a container can deliver several thousands CA molecules at a time. In addition, the nanosystem can be easily decorated with vector molecules, addressed to its targeting to specific cells or tissues, and with auxiliary components dedicated to the tailoring of its physical, chemical and biologic properties or to modify the nanoparticle behaviour. For example, nanoparticle coating with PEG or other hydrophilic appendages lead to an improvement of both solubility and plasmatic half-life, helping and extending their *in vivo* application.

This thesis reports the results of three different activities carried out during the PhD period and summarized as follows:

1) Design, synthesis and testing of three original amphiphilic MRI CAs, based on Mn^{2+}-complexes of novel lipophilic derivatives of the well know ligand EDTA. These amphiphilic chelates are included in the formulation of supramolecular lipid-based aggregates (micelles, liposomes, serum-albumin non-covalent conjugates), where they play an active role as contrast agents.

2) A unimolecular nanosized chelating agent is prepared by functionalization of polyethyleneimine with phosphonic groups. The loading of this polymeric chelating agent with Gd^{3+} ions leads to a paramagnetic nanosized system; relaxometric investigations on this system was undertaken to evaluate its potential as MRI contrast agent. The paramagnetic polynuclear complex is not intended as a component of a larger nanosized Molecular Imaging probe, rather it represents as such a complete MRI CA, containing and transporting several paramagnetic metal ions in a compact molecule of the desired nanometric size.

3) The synthetic activity of the PhD project involved the preparation of several different compounds, the latter being usually represented by polyamine-based chelating agents and their synthetic precursors. In view of the fact that most of these compounds will be employed *in vivo*, preliminary examination of their toxicity is routinely and periodically performed on the compounds prepared. During this screening, a biological activity was noticed for a family of diamines employed for the synthesis of chelating agents for Mn^{2+}, and found to be related to a block in the G1 phase of cell cycle.

Supramolecular assemblies based on amphiphilic Mn(II)-Complexes as High Relaxivity MRI probes

Mauro Botta,[a] Valeria De Biasio,[b] Giovanni B. Giovenzana,[b] Gabriele Rolla[a] and Lorenzo Tei[a]

Submitting to Chemistry - an Asian Journal

Abstract

In the field of MRI contrast agents (CAs) amphiphilic paramagnetic complexes are usually endowed with increased plasmatic half-life and high relaxivity values, but limited examples of amphiphilic Mn(II)-based CAs have been reported to date. In this work the Mn(II)-complexes of three original amphiphilic ligands derived from the well known EDTA and embodying one/two aliphatic chains were evaluated as potential MRI contrast agents and compared. Strong self-association to micelles and binding to serum albumin brought observed relaxivities to significantly high values and confirm the possibility to use supramolecular assemblies based on amphiphilic Mn(II)-complexes as high relaxivity MRI probes.

Introduction

MRI contrast agents (CAs) are paramagnetic complexes employed to increase the relaxation rate of the observed nuclei (mainly ^{1}H), allowing better diagnostic images to be acquired in a shorter period (1). Gadolinium based CAs are currently employed in clinical MRI due to the large paramagnetism showed by the f^{7}-lanthanide ion (2). Recent reports on the insurgence of pathologies associated to the release of Gd(III) ions in nephropathic patients, relived the interest in CAs based on different metal ions (3). Mn(II) represents a promising alternative (4): although magnetic properties are lower than those of Gd(III), it is an essential endogenous element and its eventual release in trace *in vivo* could be more easily managed by the organism. In addition, it is cheap and widely available. In the field of MRI CAs, amphiphilic paramagnetic complexes are usually studied in virtue of their increased plasmatic half-life and high relaxivity values, the latter being usually observed when the CAs are tightly bound to macromolecular or supramolecular systems as lipid-based formulations (5). Suitably designed lipophilic CAs can reach relaxivity values up to 90 $mM^{-1}s^{-1}$ (6) compared to the values in the range 3-5 $mM^{-1}s^{-1}$ showed by currently used "hydrophilic" CAs. While a large number of lipophilic Gd-based CAs were studied in the last two decades and summarized in recent reviews (7), scarce reports of lipophilic Mn-based CAs may be found in the scientific literature. Inclusion of the Mn(II)-complex of DTPA bis(stearylamide) in small unilamellar liposomes are the first example, dating back to 1989-90 (8); nevertheless, this system and the cognate EDTA-oleyl ester (9) recent analog represent preliminary approaches where stability issues were not tackled. Large non-hydrophilic appendages were later implanted on the backbone of the EDTA ligand to promote non-covalent interactions with serum albumin, leading to

blood-pool CAs with a significant improvement of the observed relaxivities (10, 11).

Almost all chelating agents employed for the formation of Gd(III) or Mn(II) complexes for clinical MRI applications may be classified in two families, *i.e.* acyclic and macrocyclic polyamino-polycarboxylates (12-17). As Mn-based CAs are usually endowed with lower relaxivity values compared to the corresponding Gd-based CAs, we were prompted to explore the possibility to boost their relaxometric properties by taking advantage of the formation of lipidic aggregates. To this purpose, three different ligands were synthesized, choosing the hexadentate ligands EDTA as preferred scaffold (Figure 1). The Mn(II) complexes of these newly synthesised ligands were prepared and studied by relaxometric techniques in both their aggregated form and in their supramolecular adduct with serum albumin.

Figure 1

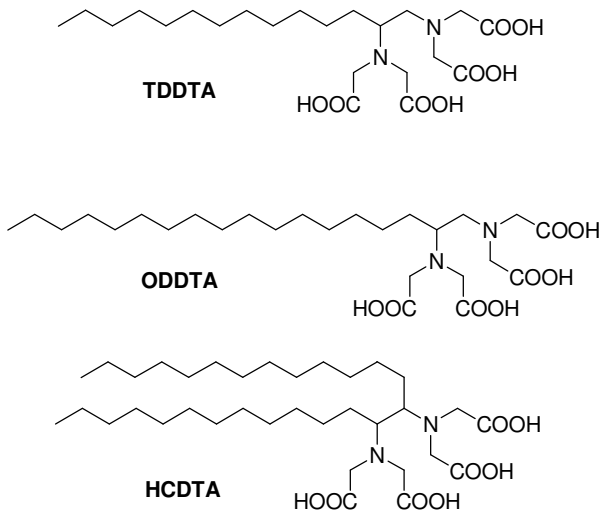

Figure 1: *Ligands synthesized in the present work.*

Results and Discussion

Ligands design

Several examples of Mn(II)-complexes with penta- or hexa-dentate polyaminopolycarboxylate ligands have been recently reported with the aim to form Mn(II)-complexes with the best balance between their thermodynamic and kinetic stabilities and the number of inner-sphere water molecules (4). Among them, Mn(II)-EDTA-like chelates still represent good systems on which build a contrast agent as Mn(II)-EDTA is well tolerated, sufficiently stable and it is has a water molecule coordinated to the metal centre (q = 1) (18). Moreover, the Mn(II)EDTA complex has the great advantage to be endowed with a water exchange rate (k_{ex}) close to an optimum value for a contrast agent (4.7×10^8 s^{-1} at 25°C). The latter property is fundamental to reach high relaxivity values once the Mn(II) complex is in a slowly tumbling form with long τ_R *i.e.* when it is in aggregated form or bound to serum albumin.

Lipophilic EDTA derivatives were designed by placing one (**TDDTA** and **ODDTA**) or two (**HCDTA**) aliphatic straight chains on the central ethylenediamine backbone, to reduce any potential steric hindrance with the metal coordination sphere. To this end, we considered the recently reported approach that used Gd-chelates bearing two aliphatic chains on adjacent coordinating arms for the formation of micelles or liposomes with the aim to reduce considerably their local rotational motion (19); with this approach, high relaxivity values up to 40 $mM^{-1}s^{-1}$ (298 K, 20 MHz) were obtained for liposomes loaded with GdDOTA$(GAC_{12})_2$. Moreover, it is well known that lipidic nanoparticles formed by amphiphilic complexes containing one aliphatic chain are not sufficiently stable in vivo giving also a strong haemolytic effect. Thus, it was shown that the presence of two aliphatic chains in the complex

allows a higher stability, a long blood half-life and no haemolytic effect. Finally, as also the length of the hydrophobic chain can influence stability, size and clearance time of the nanoparticles, twelve and sixteen carbon chains were chosen in the synthesised ligands. It is noteworthy that amphiphiles bearing C_{12} chains have been recently reported to accelerate considerably the clearance rate of liposomes embedding them in the membrane bilayer (20).

Ligands synthesis

Single chain EDTA derivatives were prepared through a common synthetic pathway, depicted in Scheme 1. 1-Tetradecene and 1-octadecene, were subjected to bromination with molecular dibromine. The vicinal dibromides were converted to the corresponding diamine through sequential conversion to the *vic*-diazide (with NaN_3 in DMF) and catalytic transfer hydrogenation (CTH) ($HCOONH_4$, Pd/C in refluxing 2-propanol). Conventional per-alkylation with *t*-butylbromoacetate/K_2CO_3 in acetonitrile and *t*-butyl esters removal with neat TFA completes the 5-steps preparation of 1,2-tetradecanediamine-*N,N,N',N'*-tetraacetic acid (**TDDTA**) and 1,2-octadecanediamine-*N,N,N',N'*-tetraacetic acid (**ODDTA**).

Scheme 1: *Synthesis of* ***TDDTA*** *and* ***ODDTA***.

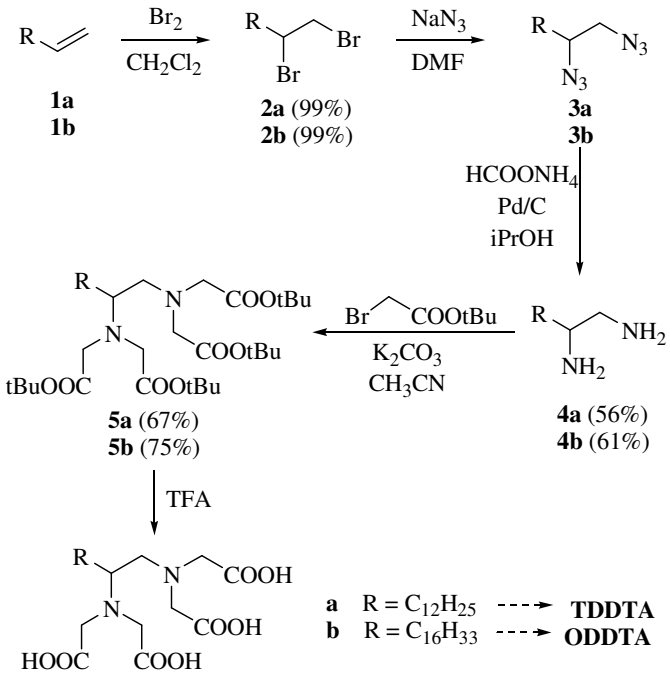

The third ligand (13,14-hexacosanediamine-*N,N,N',N'*-tetraacetic acid) (**HCDTA**) was designed to embody two aliphatic straight chains on the vicinal position of the ethylenediamine backbone. For its preparation, a different synthetic strategy was devised, reported in Scheme 2. A multicomponent condensation of 1*H*-benzotriazol, glyoxal and dibenzylamine led to a mixed diaminal (21), then reacted with 2 equivalents of dodecylmagnesium bromide giving, through a double displacement of the benzotriazole moieties, a tetrabenzylated 1,2-didodecylethylenediamine **6**. Removal of *N*-benzyl groups is accomplished by CTH to give 13,14-hexacosanediamine **7**. The primary diamine is tetraalkylated with the combination *t*-butyl bromoacetate-potassium carbonate in acetonitrile generating the tetraester **8**, subsequently converted to the final ligand **HCDTA** by treatment with neat TFA.

Scheme 2

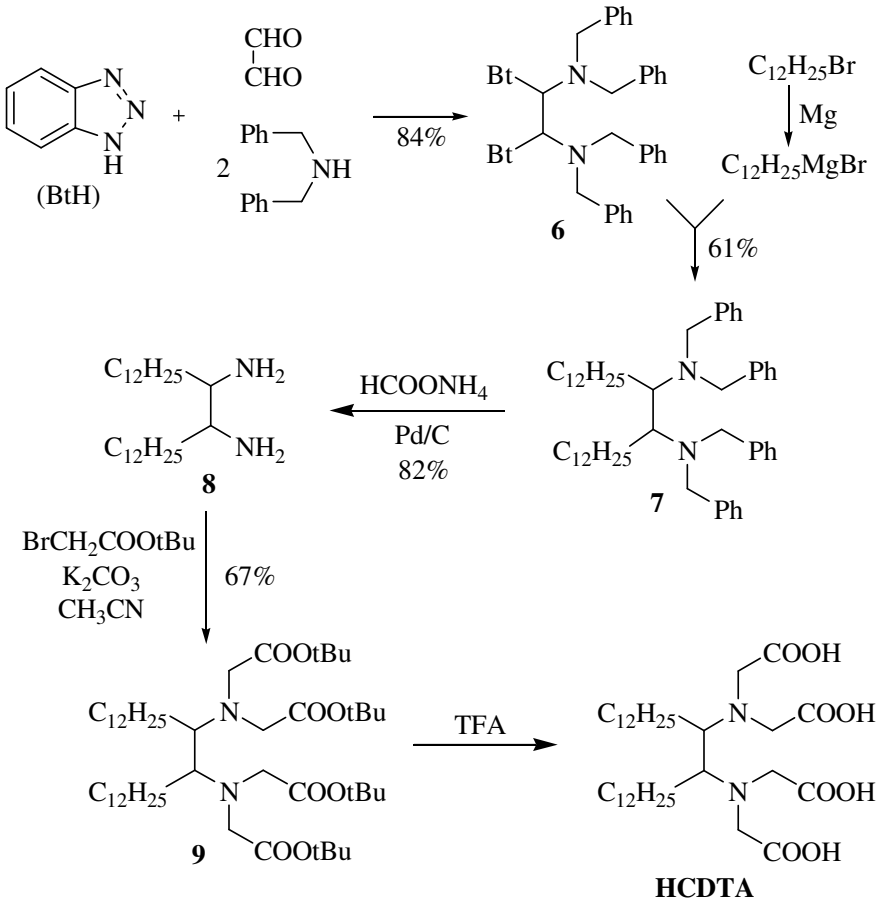

Scheme 2: *Synthetic scheme for* ***HCDTA***.

Relaxometric characterization

A detailed relaxometric characterization was undertaken on the Mn(II)-complexes prepared on the three ligands described in the previous section, in order to ascertain their potential as MRI CAs.

Determination of the relaxivity of the Mn(II)-complexes was at first accomplished on dilute solution, in order to measure relaxivity values on the monomeric form of amphiphilic complexes, *i.e.* under the critical micelle concentration above which self-aggregation may occur. The complexes Mn(II)-**TDDTA** and Mn(II)-**ODDTA** showed in these conditions relaxivities of 4.7 $mM^{-1}s^{-1}$ and 5.9 $mM^{-1}s^{-1}$, respectively, in good agreement with values expected for monomeric Mn(II)-chelate with one coordinated water molecule (q = 1). On the other side, the complex Mn(II)-**HCDTA** shows even in dilute conditions evidence of self-association and no cmc values can be determined. The relaxivity value of 18.4 $mM^{-1}s^{-1}$ measured is compatible with a supramolecular aggregate even at the lowest concentrations used for relaxivity determination. In order to establish the microscopic (supra)molecular parameters that govern the relaxivity of the complexes, their ^{1}H NMRD profiles were measured at different temperatures and concentrations ~ 1 mM.

Figure 2

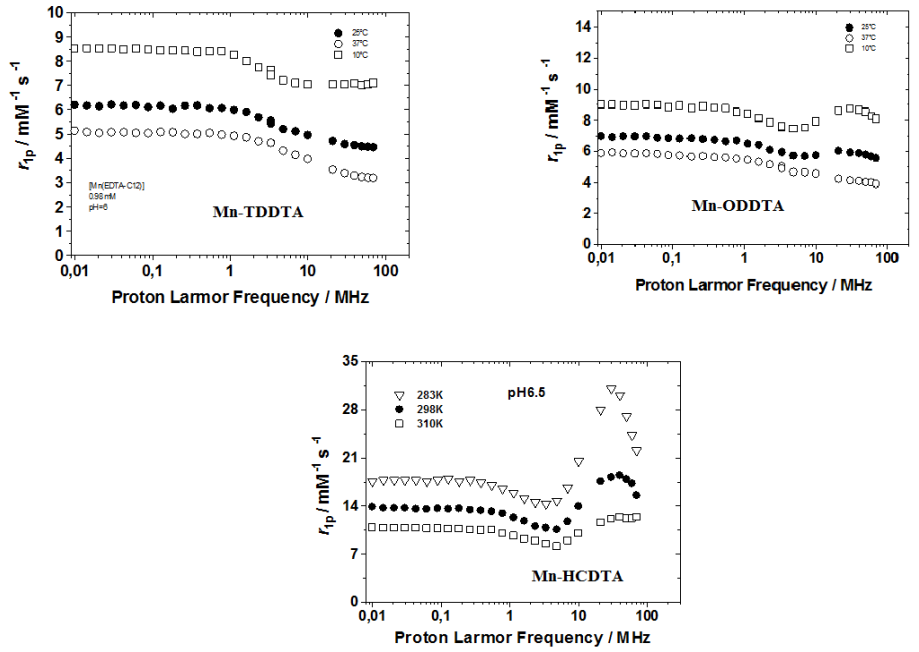

Figure 2: *NMRD profiles for Mn(II)-**TDDTA**, Mn(II)-**ODDTA**, Mn(II)-**HCDTA**.*

The results reported in Figures 2 clearly show some difference in the behaviour of the three paramagnetic species. Mn(II)-**TDDTA**, bearing a single C_{12}-aliphatic chain on the ethylenediamine backbone, show a NMRD profile quite similar to that observed for the parent EDTA. On the other hand, in the NMR profile of the longer chain analog Mn(II)-**ODDTA** a distinctive broad hump at higher fields demonstrate the formation of high-molecular weight paramagnetic species, expected in view of the concentration used (>cmc). A sharper and higher peak is observed in the NMRD profile of Mn(II)-**HCDTA**, indicative of the presence of higher-grade supramolecular aggregate than the former chelate,

further supporting the strong propensity of Mn(II)-**HCDTA** to self-association phenomena.

The NMRD profiles data at three different temperatures allow to extract information on the structural dynamics of the paramagnetic complexes. Fitting the data by the Solomon-Bloembergen-Morgan theory gives access to the parameters that influence the relaxivity, reported in Table 1.

Table 1: *Best-fit parameters obtained by analysis of the ^{1}H NMRD profiles for Mn(II)-TDDTA, Mn(II)-ODDTA, Mn(II)-HCDTA in their aggregated form.*

Parameter	**Mn(II)-TDDTA**	**Mn(II)-ODDTA**	**Mn(II)-HCDTA**
$^{298}r_{1p}$ (mM^{-1} s^{-1})[a]	4.6	5.9	18.4
Δ^2 / 10^{19} s^{-2}	10.7	8.7	1.8
$^{298}\tau_V$ / ps	23	26	33
k_{ex}^{298} / 10^6 s^{-1}[b]	470	470	470
$^{298}\tau_{RG}$ / ns	0.12	0.17	9
$^{298}\tau_{RL}$ / ps	--	--	125
S^2	--	--	0.60
q	1	1	1

R_{MnH}, a and ^{298}D were fixed in the fitting procedure to 2.83 Å, 3.6 Å and 2.3 × 10^{-5} cm^2 s^{-1}, respectively. [a] 30 MHz; [b] fixed in the fitting procedure.

The fitting shows that the three complexes share a common EDTA-like behaviour, with q = 1 and fast exchange rate of the coordinated water molecules (to be confirmed by ^{17}O NMR measurements). This is extremely useful in view

of the devised application, as the combination of a short lifetime of the coordinated water and the raise in the rotational correlation time related to the increase in the size of the paramagnetic system lead to very high values of relaxivity. Indeed Mn(II)-**HCDTA** with its significant degree of association in these conditions and shows an interesting relaxivity of 18.4 $mM^{-1}s^{-1}$, with the beneficial combination of fast water exchange and slow rotation of the paramagnetic system.

Interaction with HSA

The favourable structural and dynamic features of the EDTA-derived amphiphilic complexes pushed us to explore their behaviour in different conditions. In particular, investigation of the complexes in the presence of human serum albumin (HSA) is of great interest because this 64 KDa protein is present in high concentration in blood and its remarkable transport properties was shown to be useful for hosting paramagnetic complexes, boosting their relaxivity (6).

Relaxometric titration was then conducted on the three complexes, exposing them to increasing concentration of HSA, registering the increase in relaxivity consequent to the eventual interaction.

The results of these titrations are reported in Figure 3, along with the NMRD profiles of the complexes in the presence of an excess of HSA registered at two different temperatures (298K and 310K).

Figure 3

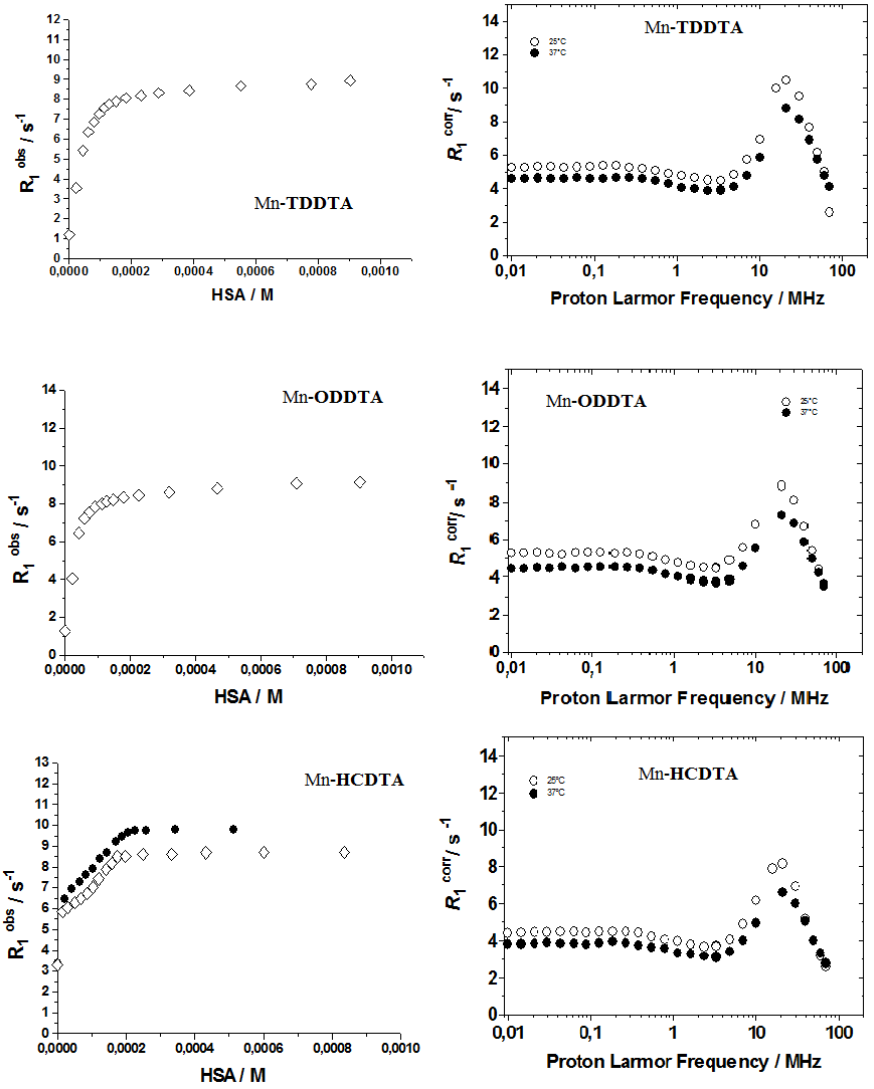

Figure 3: *Relaxometric titrations with HSA and NMRD profiles for Mn(II)-**TDDTA**, Mn(II)-**ODDTA**, Mn(II)-**HCDTA**.*

The analysis of the combined data from the titrations and the NMRD profiles allowed to extract parameters related to the interactions and to the paramagnetic system formed by the interactions of the complexes with HSA.
The results of the fitting of the data according to the SBM theory are reported in Table 2.

Table 2: *Best-fit parameters obtained by analysis of the ^{1}H NMRD profiles for the interaction of Mn(II)-**TDDTA**, Mn(II)-**ODDTA**, Mn(II)-**HCDTA** with HSA.*

Parameter	Mn(II)-**TDDTA**	Mn(II)-**ODDTA**	Mn(II)-**HCDTA**
$^{298}r_{1p}$ (mM^{-1} s^{-1})[a]	61.5	59.1	48.0
Δ^2 / 10^{19} s^{-2}	0.69	0.6	0.68
$^{298}\tau_V$ / ps	30	20	24
k_{ex}^{298} / 10^6 s^{-1}	160	160	130
$^{298}\tau_{RG}$ / ns [b]	40	40	40
$^{298}\tau_{RL}$ / ps	880	1200	261
S^2	0.72	0.70	0.66
q [b]	1	1	1

R_{MnH}, a and ^{298}D were fixed in the fitting procedure to 2.83 Å, 3.6 Å and 2.3 × 10^{-5} cm^2 s^{-1}, respectively. [a] 20 MHz; [b] fixed in the fitting procedure.

The results are very interesting as all three paramagnetic complexes efficiently interacts with the protein as can be appreciated by the curves of the relaxometric titrations. Even more astonishing are the relaxivity of the

paramagnetic systems Mn(II)-complex-HSA, towering in the range 48-61.5 $mM^{-1}s^{-1}$; these values are extremely high for this family of CAs, and rarely observed even with Gd-complexes.

The parameters of Table 2 clearly evidence that the huge increase in the relaxivity has to be ascribed to the slowed tumbling of the paramagnetic chelate as a consequence of the strong interaction with serum albumin, the latter hosting the former in one of the possible binding sites.

Additional work is in progress in order to shed more light on the nature of this strong interaction and to test these paramagnetic complexes in the presence of other molecular or supramolecular hosts.

Conclusion

In the present work, three amphiphilic ligands derived from the well known EDTA are designed and prepared. Two ligands bear a single aliphatic chain (C_{12} and C_{16}), placed on the ethylenediamine central moiety; on the same residue of the third ligand are placed in vicinal positions two identical aliphatic C_{12} chains. The Mn(II)-complexes prepared from these ligands show relaxivity values of 4.6-5.9 $mM^{-1}s^{-1}$ for the single-chain derivatives, compatible with an EDTA-like behaviour. In contrast, the double-chain derivatives shows higher relaxivity values due to self-aggregation even at the lowest concentration employed. The presence of HSA to simulate the blood environment brings a massive increase in the relaxivity, boosting to 48-61.5 $mM^{-1}s^{-1}$ as a consequence of the strong interaction of the serum protein, hosting the paramagnetic complex in a compact assembly. These results shows that Mn(II)-based CAs may be used to reach high relaxivity, usually ascribed only to Gd-based CAs, and may represent a valid and efficient alternative to the latter.

Experimental

General Information

Solvents and starting materials were purchased from Aldrich, Acros, Fluka and Alfa and used without further purification. All water solutions were prepared from ultrapure laboratory grade water (18 MΩ·cm) obtained from Millipore/MilliQ purification system. ^{1}H NMR spectra were recorded at 300 MHz with a Jeol Eclipse ECP300 spectrometer. Chemical shifts are reported in ppm with the protic impurities of the deuterated solvent as the internal reference. Mass spectra were obtained with a Finnigan LCQ-ion trap equipped with an electrospray source. TLC and gravimetric chromatography were performed with silica gel 60 (MN Kieselgel 60).

General procedure for the preparation of 1,2-dibromoalkanes

1-Alkene (1.0eq) was dissolved in dichloromethane (1 M) and bromine (1.05eq) was added dropwise to the solution until a stable red colour was obtained. The reaction mixture was further stirred at room temperature for 1 h. The solvent was removed *in vacuo* giving **2a-2b** as colourless oils, directly used for the following step.

1,2-Dibromododecane (2a)

Yield 99%.^{1}H-NMR ($CDCl_3$):4.16 (tt, 1H, *J* = 9.3, 6.8 Hz) 3.84 (dd, 1H, *J* = 10.2, 4.4 Hz), 3.61 (t, 1H, *J* = 9.9 Hz), 2.11-2.06 (m, 1H), 1.88-1.72 (m, 1H), 1.63-1.19 (m, 20H), 0.88 (bt, 3H, *J* = 6.6 Hz).^{13}C-NMR ($CDCl_3$): 53.2 (CH), 36.4 (CH_2), 36.1 (CH_2), 36.0 (CH_2), 29.76 (4xCH_2), 29.66 (CH_2), 29.51 (CH_2), 29.48 (CH_2), 28.9 (CH_2), 26.9 (CH_2), 22.8 (CH_2), 14.2 (CH_3).

1,2-Dibromooctadecane (2b)

Yield 99%. ^{1}H-NMR ($CDCl_3$): 4.15 (m, 1H), 3.83 (dd, 1H, *J*= 10.1, 4.3 Hz), 3.60 (t, 1H, *J*= 9.9 Hz), 1.87-1.74 (m, 2H), 1.62-1.16 (m, 28H), 0.89 (bt, 3H, *J*= 6.7 Hz).^{13}C-NMR ($CDCl_3$): 53.0 (CH), 36.2 (CH_2), 36.1 (CH_2), 32.1 (CH_2), 29.9 (7xCH_2), 29.7 (CH_2), 29.6 (2xCH_2), 29.0 (CH_2), 26.9 (CH_2), 22.9 (CH_2), 14.3 (CH_3).

General procedure for the preparation of 1,2-diazidoalkanes

Compounds**2a-2b** (1.0 eq) and sodium azide (3.0 eq) were dissolved in dimethylformamide (1M) and the reaction was heated to 130 °C for 2 h. Ice was added to the mixture and the pH adjusted to ~10 with NaOH. The mixture was extracted with diethyl ether (2×10 mL), and the extracts were concentrated with the help of a N_2 flow. Due to the unstable nature of diazides, compounds **3a**-**3b** were not isolated and characterized and were used as such for the following step.

General procedure for the preparation of 1,2-diaminoalkanes 4a-4b

Compounds **3a**-**3b** (1.0 eq) were slowly added dropwise into a round-bottomed flask containing triphenylphosphine (2.2 eq) and THF/diethyl ether/conc. aq NH_3(3:2:1, 0.3M) at room temperature. The reaction mixtures were the strirred at 60 °C for 3 h, then cooled, diluted with water and basified with NaOH. Extraction with diethyl ether followed by drying with Na_2SO_4, filtration and evaporation gave the crude diamines. Purification by silica-gel column chromatography (eluant toluene:2-propanol:ammonia 9:1:0.5) provided pure **4a-4b** as light yellow oils.

1,2-Dodecanediamine (4a)

Yield 56%, ^{1}H-NMR ($CDCl_3$): 2.69-2.53 (m, 2H), 2.36 (dd, 1H, *J*= 11.8, 7.8 Hz), 1.68-1.52 (m, 6H), 1.38-1.09 (m, 20H), 0.79 (bt, 3H, *J*= 5.5 Hz).^{13}C-NMR ($CDCl_3$): 53.6 (CH),48.5 (CH_2), 35.8 (CH_2), 31.9 (CH_2), 29.8 (CH_2), 29.7

(5xCH_2), 29.4 (CH_2), 26.2 (CH_2), 22.7 (CH_2), 14.1 (CH_3). ESI-MS(+): calcd for $C_{14}H_{32}N_2$: 228.3; found: 229.3 (MH^+); 251.4 (MNa^+).

1,2-Octadecanediamine (4b): Yield 61%, ^{1}H-NMR ($CDCl_3$): 2.62 (dd, 1H, *J*= 12.2, 3.7 Hz), 2.54 (m, 1H), 2.33 (dd, 1H, *J*= 12.1, 7.5 Hz), 1.33-1.08 (m, 34H), 0.77 (bt, 3H, *J*= 6.3 Hz). ^{13}C-NMR ($CDCl_3$): 53.6 (CH),48.6 (CH_2), 35.7 (CH_2), 31.9 (CH_2), 29.7-29.5 (10xCH_2), 29.3 (CH_2), 26.2 (CH_2), 22.6 (CH_2), 14.1 (CH_3). ESI-MS(+): calcd for $C_{18}H_{40}N_2$: 284.3; found: 285.5 (MH^+).

General procedure for the preparation of compounds 5a-5b: Diamines **4a-4b** (1.0 eq) were dissolved in acetonitrile (1.5 M) at room temperature. Powdered K_2CO_3 (7.0 eq) and *t*-butyl 2-bromoacetate (4.5 eq) were added to the mixtures.The reaction mixture was stirred at 60 °C for 8 h.Inorganic salts were separated by filtration and the filtrate evaporated *in vacuo*. Crude compounds **5a-5b** were purified by gravimetric chromatography (eluant petroleum ether, ethyl acetate, 2-propanol9.4:0.4:0.2), obtaining the pure tetraesters as clear light yellow viscous oils.

Tetra-*t*-butyl 1,2-dodecanediamine-*N,N,N',N'*-tetraacetate (5a): Yield 67%, ^{1}H-NMR ($CDCl_3$): 3.49-3.34 (m, 8H), 2.85 (dd, 1H, *J*= 13.2, 6.1 Hz), 2.74 (bquint, 1H, *J*= 6.1 Hz), 2.46 (dd, 1H, *J*= 13.2, 6.1 Hz), 1.42 (s, 18H), 1.41 (s, 18H), 1.37 (m, 4H), 1.27-1.16 (m, 18H),0.84 (bt, 3H, *J*= 6.4 Hz). ^{13}C-NMR ($CDCl_3$): 171.7 (C), 170.9 (C), 80.7 (C), 80.4 (C), 61.1 (CH), 56.5 (CH_2), 56.3 (CH_2), 53.3 (CH_2), 32.0 (CH_2), 30.9 (CH_2), 30.0 (CH_2), 29.7 (5xCH_2), 29.4 (CH_2), 28.22 (CH_3), 28.16 (CH_3), 27.0 (CH_2), 22.7 (CH_2), 14.1 (CH_3). ESI-MS(+): calcd for $C_{38}H_{72}N_2O_8$: 684.5; found: 685.6 (MH^+), 707.6 (MNa^+), 723.5 (MK^+), 629.5 (MH^+-*t*Bu).

Tetra-*t*-butyl 1,2-octadecanediamine-*N,N,N',N'*-tetraacetate (5b): Yield75%, ^{1}H-NMR ($CDCl_3$): 3.96 (d, 2H, *J*= 17.5 Hz), 3.85 (d, 2H, *J*= 17.5 Hz), 3.82 (d, 2H, *J*= 17.2 Hz), 3.67 (d, 2H, *J*= 17.2 Hz), 3.46-3.33 (m, 2H), 3.05 (bt, 1H), 1.45-1.12 (m, 30 H), 1.28 (s, 36 H), 0.89 (bt, 3H, *J* = 6.6 Hz).^{13}C-

NMR ($CDCl_3$): 171.4 (C), 170.6 (C), 80.5 (C), 80.1 (C), 60.9 (CH), 56.4 (CH_2), 56.2 (CH_2), 53.2 (CH_2), 31.9 (CH_2), 30.7 (CH_2), 29.8 (CH_2), 29.6 (9xCH_2), 29.3 (CH_2), 28.09 (CH_3), 28.04 (CH_3), 26.8 (CH_2), 22.6 (CH_2), 14.0 (CH_3). ESI-MS(+): calcd for $C_{42}H_{80}N_2O_8$: 740.6; found: 741.6 (MH^+), 763.7 (MNa^+), 685.6(MH^+-*t*Bu), 707.5 (MNa^+-*t*Bu).

General procedure for the preparation of the ligands DDTA and ODDTA

Compounds **5a,b** were treated with trifluoroacetic acid (10 mL) and heated to reflux for 30 min. After evaporated of volatiles, crude ligands **DDTA** and **ODDTA** were redissolved in methanol, precipitated with diethyl ether, isolated by centrifugation and washed with diethyl ether, then dried *in vacuo* obtaining the products as white solids.

1,2-Dodecanediamine-*N*,*N*,*N'*,*N'*-tetraacetic acid (DDTA)

^{1}H-NMR (CD_3OD): 3.93 (d, 2H, J = 17.5 Hz), 3.86 (d, 2H, J = 17.5 Hz), 3.80 (d, 2H, J = 17.2 Hz), 3.64 (d, 2H, J = 17.2 Hz), 3.43-3.31 (m, 2H), 3.05 (bt, 1H), 1.41-1.23 (m, 22H), 0.89 (bt, 3H, J ~ 6.7 Hz). ^{13}C-NMR (CD_3OD): 170.7 (C), 170.6 (C), 60.5 (CH), 54.5 (CH_2), 54.2 (CH_2), 52.3 (CH_2), 31.7 (CH_2), 29.42 (3xCH_2), 29.38 (2xCH_2), 29.15 (2xCH_2), 26.6 (CH_2), 26.3 (CH_2), 22.4 (CH_2), 13.1 (CH_3).

1,2-Octadecanediamine-*N*,*N*,*N'*,*N'*-tetraacetic acid (ODDTA)

^{1}H-NMR (CD_3OD): 3.95 (d, 2H, J = 17.4 Hz), 3.85 (d, 2H, J = 17.4 Hz), 3.81 (d, 2H, J = 16.8 Hz), 3.65 (d, 2H, J = 17.1 Hz), 3.45-3.28 (m, 2H), 3.04 (bt, 1H), 1.43-1.15 (m, 30H), 0.89 (bt, 3H, 6.4 Hz). ^{13}C-NMR (CD_3OD): 172.5 (C), 172.0 (C), 61.8 (CH), 55.8 (CH_2), 55.3 (CH_2), 53.6 (CH_2), 33.1 (CH_2), 30.79 (CH_2) × 7, 30.68 (CH_2) × 2, 30.5 (CH_2) × 2, 28.0 (CH_2), 27.6 (CH_2), 23.8 (CH_2), 14.4 (CH_3).

***N*,*N*,*N'*,*N'*-Tetrabenzyl-1,2-bis(benzotriazolyl)ethylenediamine (6)**

Dibenzylamine (10.01 g, 0.0507 mol) and 1*H*-benzotriazole (6.039 g, 0.0507 mol) were dissolved in ethanol (50 mL), then glyoxal (1.471 g, 0.0254 mol)

was added to the reaction mixture at room temperature. After 8 h the mixture was filtered on a Buchner funnel and the solid washed with ethanol (2 × 30 mL) and dried, obtaining 13.84 g of a yellow oil (yield 84%), solidifying on standing to a off-white waxy solid.

Synthesis of *N,N,N',N'*-tetrabenzyl-13,14-hexacosanediamine (7)

Mg turnings (2.070 g, 0.085 mol) and 1-bromododecane (19.94 g, 0.030 mol) were stirred in anhydrous tetrahydrofuran (15 mL) under nitrogen at room temperature. After 24 h compound **6** (12.013 g, 0.0369 mol) was added and the resulting grey solution stirred for 8h. The reaction mixture was filtered and evaporated *in vacuo* and the crude residue purified by gravimetric chromatography (eluant toluene), obtaining the diamine **7** as a light yellow solid (61% yield). Melting point 92.5-93.0°C. ^{1}H-NMR ($CDCl_3$): 7.39-7.19 (m, 20H), 3.65-3.53 (m, 8H), 2.79 (bt, 2H), 1.74-1.46 (m, 4H), 1.44-1.16 (m, H), 0.95 (bt, 6H, J = 6.7 Hz).^{13}C-NMR ($CDCl_3$): 140.8 (C), 128.9 (CH), 128.1 (CH),126.7 (CH), 58.5 (CH), 54.7 (CH_2), 32.1(CH_2), 30.2 (CH_2), 29.9 (4xCH_2), 29.6 (CH_2), 28.2 (CH_2), 27.1 (CH_2), 22.9 (CH_2), 14.3 (CH_3). ESI-MS(+): calcd for $C_{54}H_{80}N_2$: 756.6; found: 757.7 (MH^+).

13,14-Hexacosanediamine (8)

Ammonium formate (560.6 mg, 10.4 mmol) and Pd/C (500 mg) were dissolved in methanol (3 mL) and toluene (3 mL) under nitrogen. The tetrabenzylated diamine**7** (761 mg, 1.0 mmol) was added and the reaction was heated at refluxed for 24 h. The mixture was filtered, evaporated and partitioned between water and dichloromethane (3 × 20 mL). The crude oily product was purified by gravimetric chromatography (eluant dichloromethane/methanol, 9.6:0.4→7:3) obtaining the pure diamine**3c** (82% yield).^{1}H-NMR ($CDCl_3$): 2.52 (bt, 2H), 1.56 (bs, 4H), 1.41 (m, 4H), 1.33-1.18 (m, 40H), 0.86 (bt, 6H, J = 6.7 Hz). ^{13}C-NMR ($CDCl_3$): 55.3 (CH), 35.0 (CH_2), 32.0 (CH_2), 29.9 (CH_2), 29.7 (5xCH_2),

29.5 (CH_2), 26.7 (CH_2), 22.8 (CH_2), 14.2 (CH_3).ESI-MS(+): calcd for $C_{26}H_{56}N_2$: 396.4; found: 397.4 (MH^+).

Tetra-*t*-butyl 13,14-hexacosanediamine-*N,N,N',N'*-tetraacetate (9)

Compound **8** (2.500 g, 0.0067 mol) was dissolved in acetonitrile (40 mL) and powdered K_2CO_3 (5 eq) was added. At room temperature t-butyl 2-bromoacetate (4.2 eq) was slowly added dropwise. The reaction mixture was refluxed for 5 h, then filtered, evaporated *in vacuo* and the oily residue was purified by gravimetric chromatography (eluant 9.8:0.2 petroleum ether/ethyl acetate), obtaining a clear colorless oil. (67% yield). ^{1}H-NMR ($CDCl_3$): 3.54 (d, 4H, *J*= 16.9 Hz), 3.44 (d, 4H, *J* = 16.9 Hz), 2.57 (t, 2H, *J* = 6.0 Hz), 1.57-1.48 (m, 4H), 1.42 (s, 36H), 1.32-1.19 (m, 36H), 0.86 (bt, 6H).^{13}C-NMR ($CDCl_3$): 172.0 (C), 80.5 (C), 65.0 (CH), 54.6 (CH_2), 32.1 (CH_2), 30.0 (CH_2), 29.9 (4xCH_2), 29.5 (CH_2), 28.8 (CH_2), 28.3 (CH_3), 28.1 (CH_2), 22.8 (CH_2), 15.8 (CH_3).ESI-MS(+): calcd for $C_{50}H_{96}N_2O_8$: 852.7; found: 853.8 (MH^+), 875.8 (MNa^+), 797.7 (MH^+-*t*Bu).

13,14-Hexacosanediamine-*N,N,N',N'*-tetraaceticacid (HCDTA)

Compound **8** (3.500 g) was dissolved in trifluoroacetic acid (10 mL) and the reaction was stirred for 48 h. The solvent was evaporated and the oily residue was redissolved in methanol; slow addition of an excess of diethyl ether precipitated **HCDTA** as a white solid (1.80 g, 72% yield). Mp 186-188 °C (dec). ^{1}H-NMR (CD_3OD): 3.94 (d, 4H, *J* = 16.9 Hz), 3.75 (d, 4H, *J* = 18.1 Hz), 3.34 (m, 2H), 1.58-1.46 (m, 4H), 1.38-1.25 (m, 40H), 0.89 (bt, 6H, *J* = 6.4 Hz). ^{13}C-NMR (CD_3OD): 171.8 (C), 66.8 (CH), 54.0 (CH_2), 33.0 (CH_2), 30.8 (CH_2), 30.7 (4xCH_2), 30.6 (CH_2), 30.4 (CH_2), 30.3 (CH_2), 29.5 (CH_2), 23.6 (CH_2), 14.4 (CH_3).

^{1}H NMR Relaxation Measurements

The proton $1/T_1$ NMRD profiles were measured on a fast field-cycling Stelar SmarTracer relaxometer over a continuum of magnetic field strengths from

0.00024 to 0.25 T (corresponding to 0.01-10 MHz proton Larmor frequencies). The relaxometer operates under computer control with an absolute uncertainty in $1/T_1$ of ± 1%. Additional data points in the range 15-70 MHz were obtained on a Bruker WP80 NMR electromagnet adapted to variable-field measurements Stelar Relaxometer. The exact concentrations of gadolinium were determined by measuring the bulk magnetic susceptibility shifts of the *t*BuOH ^{1}H NMR signal on a Bruker Avance III spectrometer (11.7 T). The ^{1}H relaxation times T_1 were acquired by the standard inversion recovery method with typical 90° pulse width of 3.5 μs, 16 experiments of 4 scans. The reproducibility of the T_1 data was ±5%. The temperature was controlled with a Stelar VTC-91 (Stelar s.r.l., Mede, PV, Italy) air-flow heater equipped with a calibrated copper-constantan thermocouple (uncertainty of ±0.1°C). Variable-temperature ^{17}O NMR measurements were recorded on a Bruker Avance III spectrometer (11.74 T, 67.8 MHz for ^{17}O) equipped with a 5 mm probe and standard temperature control units. Aqueous solutions of the complexes (14.5 mM) containing 1.0% of the 17O isotope (Cambridge Isotope) were used. The observed transverse relaxation rates were calculated from the signal width at half-height.

Relaxivity was also measured with Bruker MQ20 Minispec spectrometer at 20 MHz with the "inversion recovery" method (180° - τ - 90°) by using 8 different τ values. The temperature of the sample holder was controlled with a thermostated air stream.

References

(1) a) Lauffer R B (1987), *Chem. Rev.*, **87**, 901. b) *The Chemistry of Contrast Agents in Medical Magnetic Resonance Imaging, 2nd ed.* (Eds.: A. Merbach, L. Helm, E. Toth), Wiley, New York, 2013.

(2) a) Caravan P, Ellison J J, McMurryn T J, Lauffer R B (1999), *Chem. Re*v., **99**, 2293. b) Geraldes C F G C, Laurent S (2009), *Contrast Media Mol. Imaging*, **4**, 1.

(3) a) Kuo P H, Abu-Alfa A, Bucala R, Griffith J, Carlson K, Girardi M, Weinreb J, Cowper S (2009), *Appl. Radiology*, **38**, 22-33. b) Kribben A, Witzke O, Hillen U, Barkhausen J, Daul A E, Erbel R (2009), *J. Am. Coll. Radiol.*, **53**, 1621-1628. c) Morcos S K, Haylor J (2010), *World J. Radiol.*, **2**, 427-433.

(4) a) Pan D, Schmieder A H, Wickline S A, Lanza G M (2011), *Tetrahedron*, **67**, 8431-8444. b) Kueny-Stotz M, Garofalo A, Felder-Flesch D (2012), *Eur. J. Inorg. Chem.*, 1987-2005.

(5) Botta M, Tei L (2012), *Eur. J. Inorg. Chem.*, 1945-1960.

(6) Gianolio E, Giovenzana G B, Longo D, Longo I, Menegotto I, Aime S (2007), *Chem. Eur. J.*, **13**, 5785-5797.

(7) Accardo A, Tesauro D, Aloj L, Pedone C, Morelli G (2009), *Coord. Chem. Rev.*, **253**, 2193-2213.

(8) a) Schwendener R A, Wüthrich R, Duewell S, Westera G, von Schultess G K (1989), *Int. J. Pharm.*, **49**, 249-259. b) Schwendener R A, Wüthrich R, Duewell S, Wehrli E, Schultess D K (1990), *Invest. Radiol.*, **25**, 922-932. c) Unger E, Fritz T, Shen D K, Wu G (1993), *Invest. Radiol.*, **28**, 933-938.

(9) Moghaddam M J, de Campo L, Waddington L J, Weerawardena A, Kirby N, Drummond C J (2011), *Soft Matter*, **7**, 10994-11005.

(10) Aime S, Anelli P L, Botta M, Brocchetta M, Canton S, Fedeli F, Gianolio

E, Terreno E (2002), *J. Biol. Inorg. Chem.*, **7**, 58–67.

(11) Troughton J S, Greenfield M T, Greenwood J M, Dumas S, Wiethoff A J, Wang J, Spiller M, McMurry T J, Caravan P (2004), *Inorg. Chem.*, **43**, 6313.

(12) Zhang Q, Gorden J D, Beyers R J, Goldsmith C R (2011), *Inorg. Chem.*, **50**, 9365.

(13) de Sá A, Bonnet C, Geraldes C F G C, Tóth E, Ferreira P M T, André J P (2013), *Dalton Trans.*, **42**, 4522.

(14) Drahoš B, Pniok M, Havlíčková J, Kotek J, Císařová I, Hermann P, Lukeš I, Tóth E (2011), *Dalton Trans.*, **40**, 10131

(15) Drahoš B, Kotek J, Císařová I, Hermann P, Helm L, Lukeš I, Tóth E (2011), *Inorg. Chem.*, **50**, 12785.

(16) Drahoš B, Kotek J, Hermann P, Lukeš I, Tóth E (2010), *Inorg. Chem.*, **49**, 3224.

(17) Su H, Wu C, Zhu J, Miao T, Wang D, Xia C, Zhao X, Gong Q, Song B, Ai H (2012), *Dalton Trans.*, **41**, 14480.

(18) Wang X F, Gao J, Wang J, Zhang Zh H, Wang Y F, Chen L J, Sun W, Zhang X D (2008), *J. Struct. Chem.*, **49**, 724.

(19) Kielar F, Tei L, Terreno E, Botta M (2010), *J. Am. Chem. Soc.*, **132**, 7836.

(20) Cittadino E, Botta M, Tei L, Kielar F, Stefania R, Chiavazza E, Aime E, Terreno E (2013), *ChemPlusChem*, **78**, 712.

(21) Katritzky A R, Fan W Q, Fu C (1990), *J. Org. Chem.*, **55**, 3209.

Phosphonated polyethyleneimine (PEI-P): evaluation of a chelating polymer as a unimolecular nanosized MRI contrast agents

Authors: Silvio Aime,[a] Eliana Gianolio,[a] Giovanni B. Giovenzana[a,b] and Valeria De Biasio[b]

Submitting to RSC Advances

Abstract

A unimolecular nanosized chelating agent (PEI-P) is prepared by functionalization of polyethyleneimine with phosphonic groups. The loading of PEI-P with Gd^{3+} ions leads to a paramagnetic nanosized system; relaxometric investigations on this system was undertaken to evaluate its potential as MRI contrast agent.

Introduction

Paramagnetic systems are currently employed as MRI contrast agents (CAs), to increase the relaxation rate of the observed nuclei (mainly ^{1}H) and allowing to acquire better diagnostic images in a shorter period (1).

Different families of paramagnetic systems were developed in the last 30 years to achieve high relaxation properties, combined with thermodynamic and

kinetic stability needed for a safe *in vivo* use (2).

Small Gd^{3+} chelates dominate the clinical MRI CAs market, and are widely employed in a significant proportion of all MRI examinations; superparamagnetic iron oxide nanoparticles have been used as "negative" CAs (3).

The low sensitivity of MRI compared to other imaging techniques drove an intensive search for high relaxivity MRI CAs (relaxivity is defined as the increase of the relaxation rate of 1H nuclei of a 1 mM solution of the CA). Improvements in the family of Gd^{3+} chelates was accomplished mainly through: i) raising in the number ("*q*") of coordinated water molecules (fighting to maintain a suitable complex stability) (4); ii) increasing the number of paramagnetic metal ions, e.g. by using polynuclear complexes; iii) slowing the rotational tumbling rate of the paramagnetic chelate (5), by inclusion (6), interaction (7) or link with a macromolecular system such as proteins, polymers (8), dendrimers (9) and nanoparticles (10).

The latter strategy usually relies on the preliminary preparation of Gd^{3+}-chelate incorporating a free functional group, subsequently used for conjugation to the selected macromolecule. The drawback of this approach is the need for a bifunctional chelating agent (BFCA) (11) and the possibility that a flexible linkage between the metal complex and the macromolecule can leave the paramagnetic chelate free to rotate, vanifying the devised reduction of its rotational rate.

We envisage that the use of the backbone atoms of a polymeric macromolecule to coordinate metal ions can lead to significant improvements of this strategy: i) avoiding expensive BFCAs or their lenghty preparations, ii) tightly embracing the paramagnetic metal ions in the slowly moving macromolecule; iii) exploiting the polymeric nature of the macromolecule to bind several metal ions into a unimolecular nanosized system.

In this manuscript we describe the preparation of a polymeric chelating agent and the corresponding Gd^{3+} complex (**PEI-P**, Scheme 1), and the evaluation of its behaviour as a potential MRI CA through a detailed relaxometric study.

Scheme 1

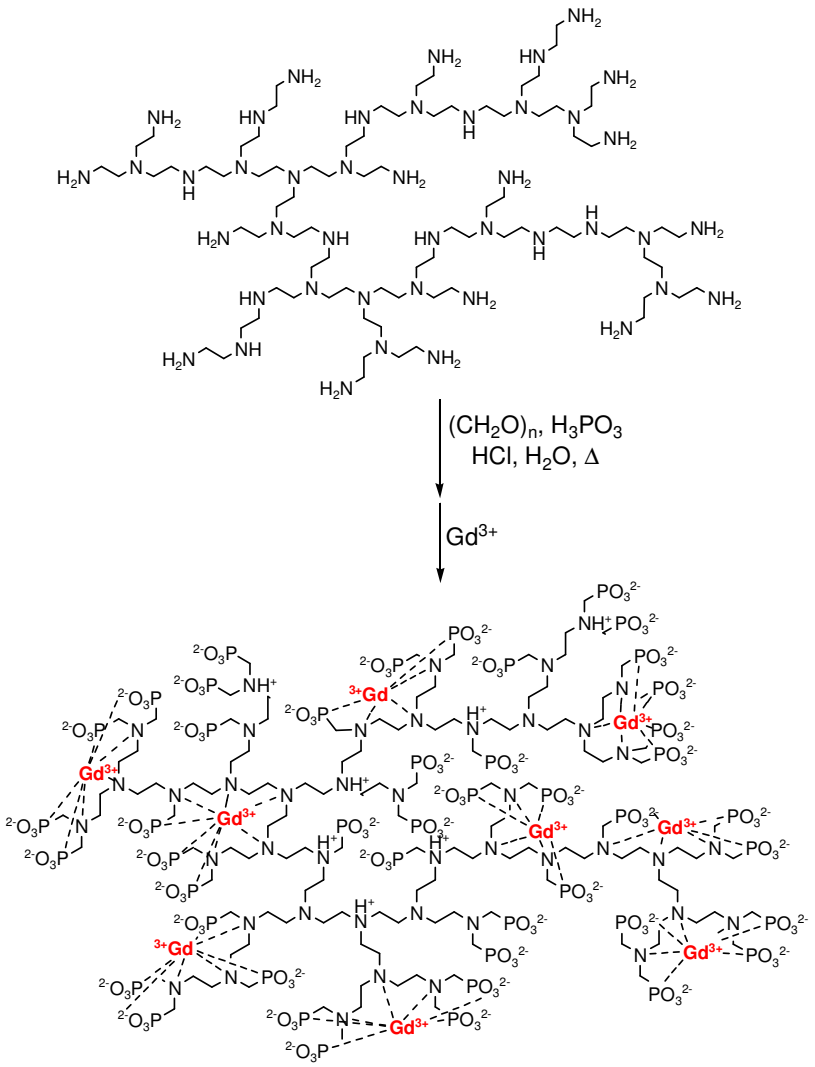

Scheme 1: *Preparation of PEI-P-Gd^{3+} (idealized average structure of the starting material and product; coordinated water molecules omitted for clarity).*

Commercially available low MW polyethyleneimine (**PEI**) was chosen as preferred scaffold to build the polymeric chelating agent for several different reasons: i) amino groups in the polymer backbone may play both a structural and a coordinating role; ii) primary and secondary amino groups may be easily functionalized with coordinating groups, targeting moieties or tailoring residues; iii) the ethylene spacer between two nitrogen atoms allows metal chelation through the formation of stable five-membered rings; iv) **PEI** is a freely water soluble and cheap starting material. Phosponate coordinating groups were introduced by an adaptation of the classical Moedritzer-Irani protocol (12).

Previous example of functionalized **PEI** as a coordinating polymer may be found in the removal of toxic metal ions (13), while a phosphonated high molecular weight derivative was employed to bind ^{99m}Tc and ^{153}Sm as potential therapeutic radiopharmaceuticals (14). In the field of MRI CAs, a **PEI** grafted with macrocyclic chelating agents was reported (15), but in this system the polymer do not actively participate in the coordination of the metal ion but simply as a macromolecular scaffold.

Experimental

General: Reagents and dialysis tubes were obtained from Aldrich and used without further purification. All water solutions were prepared from ultrapure laboratory grade water (18 MΩ·cm) obtained from Millipore/MilliQ purification system.

Preparation of functionalized polyethyleneimine (PEI-P)

Polyethyleneimine (MW 1800-2000, 50% aq solution, 10.00 g) was dissolved in water (10 mL) and conc. HCl was added until pH 1. Phosphorous acid (12.32

g) was added in one portion and the resulting mixture was brought to reflux. Paraformaldehyde (7.51 g) was added portionwise during 1 h, then the mixture was refluxed for 8 h and left overnight at room temperature. Concentration *in vacuo* to approx half volume, followed by slow addition of excess ethanol induced precipitation of a off-white gummy product, isolated by decantation and washed with ethanol. The crude product was redissolved in the minimum volume of conc. HCl/H_2O 1:1 and reprecipitated by slow addition of an excess ethanol, followed by decantation and repeated washing with ethanol. Exhaustive elimination of low molecular weight reagents and byproducts was accomplished through extensive dialysis against water (benzoylated dialysis tubes, MW cut-off 2000, 5 cycles). The retentate was evaporated to dryness giving PEI-P (13.97 g). ^{1}H-NMR (D_2O, 300 MHz, 333K): 4.05-2.95 (br s). ^{13}C-NMR (D_2O, 75.4 MHz, 333K): 56.0-52.5 (br, CH_2), 56.0-48.7 (br, CH_2), 46.3-44.8 (br, CH_2). ^{31}P-NMR (D_2O, 121.4 MHz, 333K): 20.1-7.2 (br s).

Preparation of the Gd-PEI-P complex

PEI-P (1.569 g) was dissolved in water (15 mL) and gadolinium hydroxide (freshly precipitated with NaOH 1M from an aqueous solution containing 1.997 g $GdCl_3$, centrifuged and washed with distilled water). The suspension was stirred at room temperature overnight and for additional 2 h at 60°C and then filtered. The filtrate was dialyzed (benzoylated dialysis tubes, MW cut-off 2000) against: i) water (1 cycle); ii) EDTA disodium (25 mM, pH 7) (5 cycles), to remove loosely bound Gd^{3+} ions; iii) water (3 cycles). The retentate was lyophilized to give Gd-PEI-P (1.763 g) as a white powder.

Relaxometric Characterization

The longitudinal water proton relaxation rate as a function of the pH was measured by using a Stelar Spinmaster (Stelar, Mede, Pavia, Italy) spectrometer operating at 20 MHz, by means of the standard inversion–recovery technique. The temperature was controlled with a Stelar VTC-91 airflow heater equipped

with a copper-constantan thermocouple (uncertainty 0.1 °C). The proton $1/T_1$ NMRD profiles were measured over a continuum of magnetic field strength from 0.00024 to 0.47 T (corresponding to 0.01−20 MHz proton Larmor frequencies) on a Stelar field-cycling relaxometer. The relaxometer works under complete computer control with an absolute uncertainty in $1/T_1$ of 1%. Data points from 0.47 T (20 MHz) to 1.7 T (70 MHz) were collected on a Stelar Spinmaster spectrometer working at variable field. The concentration of the gadolinium complex solutions, for relaxometric characterization, was determined by mineralizing a given quantity of the sample solution by the addition of 37% HCl at 120°C overnight. From measurement of the observed relaxation rate (R_{1obs}) of the acidic solution and knowing the relaxivity (r_{1p}) of Gd^{3+} aquaion in acidic conditions (13.5 $mM^{-1}s^{-1}$), it was possible to calculate the exact gadolinium(III) concentration (this method was calibrated using standard ICP solutions, and the accuracy was determined to be <1%).

Results and discussion

Relaxometric properties

Relxometric investigations on Gd-**PEI-P** were performed on 1 mM solutions prepared in isotonic phosphate buffered saline (PBS). Solutions of Gd-**PEI-P** in water showed aggregation phenomena leading to partial precipitation of the polymer and suggesting a stabilizing role of counterions with respect to the polymer charges. Absence of free Gd^{3+} ions was checked by UV-Vis spectrophotometric analysis with Xylenol Orange (16).

The relaxivity value was determined to be 10.7 $mM^{-1}s^{-1}$ in PBS (pH 7.0, 25°C, 20 MHz) and linear in the range of concentration 0-5 mM. A higher value of 14.9 $mM^{-1}s^{-1}$ was registered in water although this enhancement could be

attributed to the formation of high molecular weight aggregates with a reduced rotational rate and finally leading to the above cited precipitation. Assuming the idealized structure of Scheme 1 for the polymeric chelate, containing an extimated number of 7-9 Gd^{3+} ions, an attractive overall relaxivity of 75-96 $mM^{-1}s^{-1}$ could be calculated for each nanosized unimolecular system, one order of magnitude higher than the values showed by clinically employed Gd^{3+}-complexes (4-6 $mM^{-1}s^{-1}$).

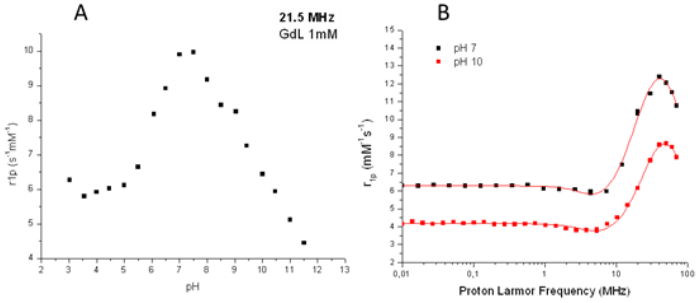

Figure 1: *A) Relaxivity vs pH for Gd-**PEI-P**, 21.5 MHz. B) NMRD profiles registered for Gd-**PEI-P** at neutral and basic pH.*

The relaxivity of Gd-**PEI-P** was studied as a function of pH (Fig. 1A), revealing an unusual behaviour. The paramagnetic system shows an asymmetric bell-shaped trend, with the relaxivity peaking around pH 7. The decrease in the relaxivity observed at acidic pH is related to the partial precipitation, likely induced by protonation-driven formation of larger aggregates; on the other side, basic pH values lead to a monotonic reduction of relaxivity, attributed to the displacement of coordinated water molecules by anions such as hydroxide, phosphate or adventitious carbonate.

The composite behaviour of the relaxivity of Gd-**PEI-P** on varying the pH prompted us to explore in detail the mechanisms involved. NMRD profiles of Gd-**PEI-P** at neutral and acidic pH were registered and are reported in Fig. 1B; both NMRD profiles show a peak of relaxivity centered around 50 MHz, typically observed in slowly rotating systems.

The ^{17}O NMR R_2 values of Gd-**PEI-P** were determined at 14.1 T in the temperature range 5-70°C (Fig. 2B). The experimental data show a nearly exponential increase with decreasing temperature, indicating the occurrence of a fast exchange regime for the coordinated water molecule(s), even if the comparison with Gd-**DO3A** and Gd-**DOTA** where the coordinated water molecules are respectively 2 and 1, clearly shows a lower level of hydration in the inner coordination sphere of the metal centers of the polynuclear complex.

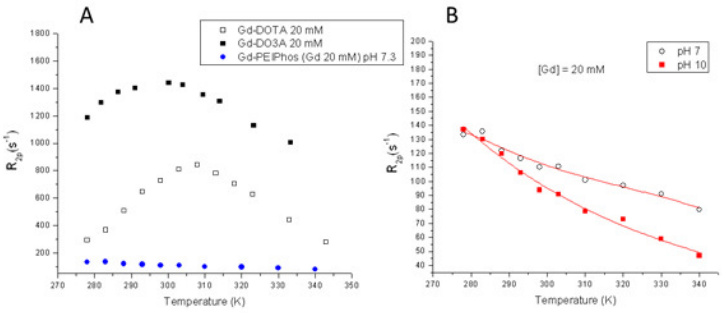

Figure 2: *A) ^{17}O NMR R_2 of Gd-**PEI-P** compared to Gd-**DO3A** and Gd-**DOTA**. B) ^{17}O NMR R_2 of Gd-**PEI-P** at neutral and basic pH.*

The ^{17}O NMR spectroscopic data were analyzed in terms of the Swift-Connick equations (17), whereas the NMRD profiles were fitted to the standard equations for the inner- (IS) and outer-sphere (OS) relaxation contributions.

The results of the fitting procedure are summarized in Table 1.

Table 1 Parameters obtained from the fitting of NMRD profiles and ^{17}O NMR data for Gd-**PEI-P**.

Gd-**PEI-P**	τ_M[a] (ns)	τ_R (ns)	q	τ_V (ps)	Δ^2 (s^{-2})
PBS pH 7.3	88	1.71 ±0.17	0.31 ±0.010	34.7 ±0.82	$(2.71\pm0.07)\cdot10^{19}$
PBS pH 10.0	88	1.88 ±0.14	0.22 ±0.007	27.5 ±0.47	$(4.03\pm0.11)\cdot10^{19}$

[a] Obtained from ^{17}O NMR data.

The fast exchange regime of the coordinated water molecules is demonstrated by their exchange lifetime, located under 100 ns from ^{17}O NMR data. The significantly high value of τ_R, close to 2 ns, can be easily ascribed to the nanometric size of the system, clearly fulfilling the task to include multiple paramagnetic metal centers in a slowly rotating context.

The favorable combination of these parameters explains the >10 $mM^{-1}s^{-1}$ values of observed relaxivities at the bell apex, that associated with the presence of multiple Gd^{3+} ion in the molecular system lead to a nanosized CA with attractive performances, especially in the 50-60 MHz region where a large portion of the clinical MRI scanner operate.

Stability evaluation

Stability issues ensuing from the observation of diseases related to chelate dissociation (18) require a mandatory evaluation of the stability of Gd^{3+}-complexes. Even if kinetic factors may strongly influence the behaviour of the complex, thermodynamic stabilities with Log $K_{Gd\text{-}L}$ well over 20 are usually

needed to avoid the release of the Gd^{3+} ion under physiological conditions.

Relaxometric data indicates that the metal centers coordinates only 0-1 molecules of waters: it is reasonable to expect that the lanthanide metal ions, usually accomodating 8-9 donor groups in their inner sphere, are coordinated in this system by a number of functional groups ranging from 7 to 9. Either amino groups of the PEI backbone or phosphonic groups may contribute to the coordination, provided that they are suitably placed, either by connectivity or by spatial proximity. The strong participation of the polymeric ligand to the coordination of the metal ions may be likely ascribed to the preliminary selection operated by elimination of loosely bound Gd^{3+} ions by extensive dialysis against EDTA (hence "loosely bound" is to be intended as "bound with a formation constant lower than Gd-EDTA").

The heterogeneous nature of the polymeric system studied in this work implies that the metal ions included in the polychelating matrix experience different coordinating environments, determined by the several possible combination of amino and phosphonic groups. This precludes the determination of *accurate* formation constants for the single coordinating arrangements. Nevertheless, an extimation of an *average* formation constant could be useful to assess the overall stability of the system as a whole.

To this purpose, competition experiments were performed, tackling Gd-**PEI-P** with ligands as EDTA and DTPA, for which the formation constant of the corresponding Gd-complexes are known. The relaxivity of a 1 mM solution of Gd-**PEI-P** was measured after the addition of increasing amounts of EDTA or DTPA (Fig. 3).

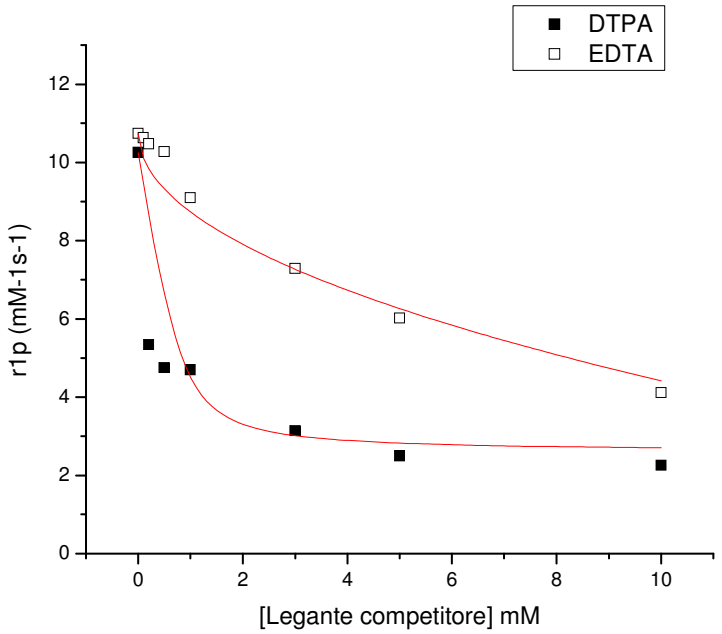

Figure 3: *Relaxometric titration of Gd-**PEI-P** with EDTA and DTPA (20 MHz, 298K.)*

Fitting the results with the literature values of $K_{Gd\text{-}EDTA}$ and $K_{Gd\text{-}DOTA}$ allowed to obtain an average value of the formation constant Log $K_{Gd\text{-}\mathbf{PEI\text{-}P}}$ = 21.6, noticeably higher than the safety limit previously stated.

Interaction with meglumine

The unusual behaviour registered for Gd-**PEI-P** on varying the pH led us to explore the possibility to modify the solution properties of the unimolecular nanosized CAs. The idealized structure of Gd-**PEI-P** depicted in Scheme 1 shows that the outer surface contains a large number of phosphonic groups, some of them involved in the metal complexation and some other free. The ionization of these groups leads to an overall negative charge of the surface: preliminary measurements provided Z-potential values ranging from -20 ÷ -30

mV, indicating that the phosphonates negative charge largely overcomes the positive charges of the protonated amines of the PEI backbone.

We decided then to use meglumine (*N*-methylglucamine) as a cationic surface modifier. The use of this biocompatible and highly hydrophilic amine was already described to increase the relaxometric properties of a negatively charged CA, in virtue of the formation of an ion pair, leading to a large increase of the second sphere hydration of the metal complex (19). In our intention, meglumine could be beneficial for Gd-**PEI-P**: i) exerting a protective effect against aggregation; ii) improving the solubility profile of the nanosized system; iii) enhancing the relaxivity of the exposed metal ions through the hydration boosting mechanism reported previously.

Relaxometric titration of a Gd-**PEI-P** solution with meglumine (Fig. 4) shows the expected improvement of relaxivity, growing from 10.7 $mM^{-1}s^{-1}$ towards a saturation value of ~ 12 $mM^{-1}s^{-1}$ and supporting the alleged surface coverage by electrostatic interaction.

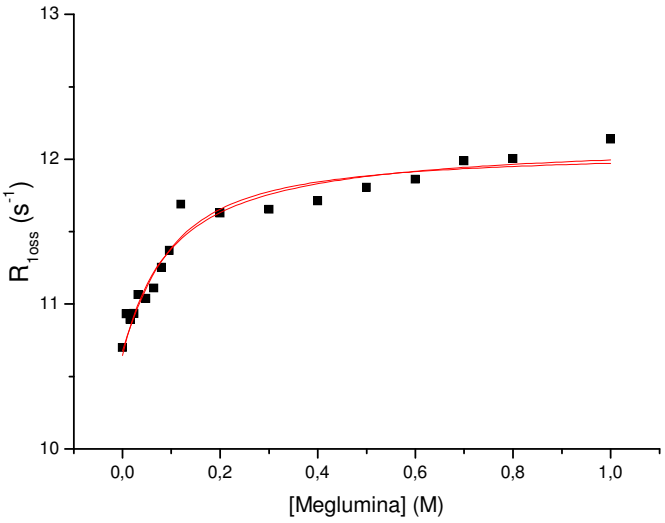

Figure 4: *Relaxometric titration of Gd-**PEI-P** with meglumine (20 MHz, 298K).*

The shielding effect of the meglumine coating becomes apparent with the determination of the relaxivity as a function of pH for the supramolecular adduct (Fig. 5), where the relaxivity fall observed at basic pH values of the asymmetric bell-shaped behaviour of pristine Gd-**PEI-P** is completely removed, with relaxivity being approximately unchanged in the pH range 8-12.5.

A less pronounced effect is observed even at acidic pH values, where the relaxivity decrease is shifted leftwards of ~ 1 pH unit, further widening the stability window of the system.

Meglumine plays then a double shielding role, either against the coordinating anions adversely affecting the relaxivity at basic pH, or preventing the aggregation by self-complementary electrostatic interaction operating at acidic pH.

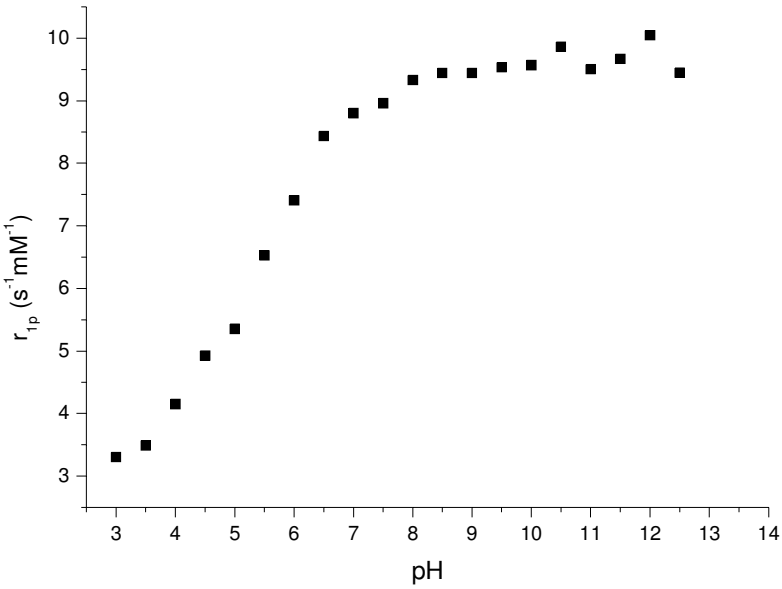

Figure 5: *Relaxivity vs pH for meglumine-coated Gd-**PEI-P** ([Gd-**PEI-P**]=70 μM, [meglumine]=100mM, 20 MHz, 298K).*

A third shielding effect was finally observed when tackling the thermodynamic stability of meglumine-coated Gd-**PEI-P** with DTPA in the same conditions employed for the relaxometric titration reported in Fig. 3. It was indeed observed (Fig. 6) that higher concentration of DTPA (roughly threefold) are needed to remove the metal ions from meglumine-coated Gd-**PEI-P** compared to native Gd-**PEI-P**, paving the way to an increase in the safety profile of this interesting nanosized CA.

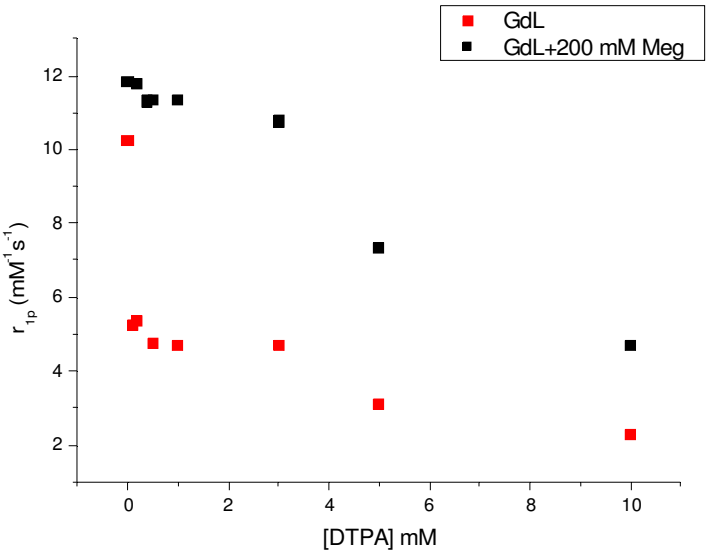

Figure 6: *Comparison of the relaxometric titration of meglumine-coated and native Gd-**PEI-P** (20 MHz, 298K).*

Conclusions

In conclusion we reported the preparation of an original unimolecular nanosized Gd-based contrast agent for MRI (Gd-**PEI-P**), based on polyethyleneimine functionalized with phosphonate groups. Relaxometric investigation highlighted an unusual behaviour of this paramagnetic system, with a remarkable relaxivity, the latter varying with an asymmetric bell-shaped profile as a function of pH. The high relaxivity value was attributed through NMRD and ^{17}O NMR measurements to a favourable combination of a fast exchange of coordinated water molecule on the metal centers and the slow rotation imposed

to the system by its unimolecular nanosized structure. Competition experiments with known ligand showed a noteworthy thermodynamic stability of the polychelate.

Significant improvements of the relaxometric properties and the stability profiles of Gd-**PEI-P** was obtained by interaction with meglumine, acting as a cationc surface modifier and binding to the exposed anionic phosphonate groups.

References

1 Lauffer R B (1987), *Chem. Re*v., **87**, 901.

2 Geraldes C F G C, Laurent S (2009), *Contrast Media Mol. Imaging*, **4**, 1.

3 Caravan P, Ellison J J, McMurry T J, Lauffer R B (1999), *Chem. Re*v., **99**, 2293.

4 a) Datta A, Raymond K N (2009), *Acc. Chem. Res.*, **42**, 938; b) Aime S, Calabi L, Cavallotti C, Gianolio E, Giovenzana G B, Losi P, Maiocchi A, Palmisano G, Sisti M (2004), *Inorg. Chem.*, **43**, 7588.

5 a) Aime S, Botta M, Fasano M, Geninatti Crich S, Terreno E (1996), *J. Biol. Inorg. Chem.*, **1**, 312; b) Lauffer R B, Parmelee D J, Dunham S U, Ouellet H S, Dolan R P, Witte S, McMurry T J, Walovitch R C (1998), *Radiology*, **207**, 529.

6 a) Aime S, Botta M, Garino E, Geninatti Crich S, Giovenzana G B, Pagliarin R, Palmisano G, Sisti M (2000), *Chem. Eur. J.*, **6**, 2609; b) Aime S, Botta M, Fedeli F, Gianolio E, Terreno E, Anelli P (2001), *Chem. Eur. J.*, **7**, 5262.

7 a) Gianolio E, Giovenzana G B, Longo D, Longo I, Menegotto I, Aime S (2007), *Chem. Eur. J.*, **13**, 5785; b) Briley-Saebo K C, Geninatti S, Barazza A, Cormode D, Mulder W J M, Chen W, Giovenzana G B, Aime S, Fayad Z A (2009), *J. Phys. Chem. B*, **113**, 6283.

8 a) Aime S, Botta M, Geninatti Crich S, Giovenzana G B, Palmisano G, Sisti M (1999), *Chem. Commun.*, **16**, 1577; b) Grogna M, Cloots R, Luxen A, Jérôme C, Desreux J F, Detrembleur C (2011), *J. Mater. Chem.*, **21**, 12917.

9 a) Xu H, Regino C A S, Bernardo M, Koyama Y, Kobayashi H, Choyke P L, Brechbieln W M (2007), *J. Med. Chem.*, **50**, 3185; b) Rudovskỳ J, Botta M, Hermann P, Hardcastle K I, Lukeš I, Aime S (2006), *Bioconjugate Chem.*, **17**, 975.

10 Mulder W J M, Strijkers G J, Van Tilborg G A F, Cormode D P, Fayad Z A, Nicolay K (2009), *Acc. Chem. Res.*, **42**, 904.

11 Lattuada L, Barge A, Cravotto G, Giovenzana G B, Tei L (2011), *Chem. Soc. Rev*., **40,** 3019.

12 Moedritzer K, Irani R R (1966), *J. Org. Chem.*, **31**, 1603.

13 Wang G, Chang Q, Zhang M, Han X (2013), *React. Funct. Polym.*, **73**, 1439.

14 Jarvis N, Zeevaart J R, Wagener J M, Louw W K A, Dormehl I C, Milner R J, Killian E (2002), *Radiochim. Acta*, **90**, 237.

15 Jászberényi Z, Moriggi L, Schmidt P, Weidensteiner C, Kneuer R, Merbach A E, Helm L, Tòth E (2007), *J. Biol. Inorg. Chem.*, **12**, 406.

16 Barge A, Cravotto G, Gianolio E, Fedeli F (2006), *Contrast Med. Mol. Imaging*, **1**, 184.

17 Swift T J, Connick R E (1962), *J. Chem. Phys.*, **37**, 307.

18 a) Thomsen H S, Morcos S K, Dawson P (2006), *Clin. Radiol.*, **61**, 905; b) Aime S, Caravan P (2009), *J. Magn. Res. Imaging*, **30**, 1259.

19 Aime S, Botta M, Terreno E, Anelli P L, Uggeri F (1993), *Magn. Res. Med.*, **30**, 583.

N-Polybenzylated Alicyclic 1,2-Diamines Show Cytotoxicity and G1 Phase Arrest in Cancer Cell Line

Authors: Antonio Caldarelli,[a] Valeria De Biasio,[a] Giovanni B. Giovenzana,[a] Gianpiero Mastronardo,[a] and Roberto Negri[a*]

Submitted in *Molecular Diversity*, manuscript number MODI-DI-13-00237R1

Abstract

Citotoxicity in the μM range was observed in cancer cell lines treated with *N,N,N',N'*-tetrabenzyl-4,5-diamino-2-cyclopentenone. Cell cycle analysis on HeLa cells showed a clear G1 phase arrest. A preliminary SAR on structural analogs was performed in order to identify the pharmacophores.

Introduction

Cancer is currently one of the most relevant causes of death (1, 2). Identification of new compounds to be used in oncological therapy is nowadays one of the greatest challenges for medicinal chemists. Improvement of known active compounds is an immediate strategy to find new drugs to be tested in clinical trials. Screening of known compounds for unknown bioactivities is an alternative approach; it can help to identify new lead compounds and it is made

easier by the usually larger availability of the chemicals and of the information about their chemical properties, synthesis and reactivity.

The majority of all drugs contains amine groups, hence we focused our attention on synthetic amines, and particularly on 1,2-diamines. The 1,2-diamino moiety can be found in many natural and synthetic substances showing valuable biological properties (3, 4). Among them is possible to cite, for instance, antidepressant agents (5), antiarrhythmics (6), antimicrobial (7), antiparasitic against *Leishmania* spp and *Trypanosoma cruzi* (8, 9) and anticancer drugs. Antitumoral properties of cisplatin (10) and its success in chemotherapy brought about the synthesis of many diamino-platinum complexes with improved properties, as oxaliplatin and DWA 2114R. Several 1,2-diamino-platinum complexes were prepared and tested for antitumoral activity, making these compounds the most popular examples of 1,2-diamino moiety in medicinal chemistry (11-17). Few others "non-metallic" compounds possessing the 1,2-diamine moiety showed anticancer activity, too. Bis-naphthalimides linked by an ethylenediamine moiety, like DMP 840, showed an excellent activity against several human tumor xenografts in mice (18, 19). Balanol, a natural compound extracted from the fungus *Verticillum balanoides*, was found to be a potent inhibitor of PKC (protein kinase C), the latter playing a key role in cell growth, metabolism and differentiation (20).

During our search of synthetic approach to vicinal diamines we were intrigued by the recent interest on a RORC (Ring-Opening/Ring-Closure) reaction between furfural and secondary amines (21-25). Stenhouse explored this reaction with aromatic amines in presence of acidic catalysts more than 150 years ago, in order to obtain compounds with dye properties (26-29). Noticing that no biological studies of this interesting structure have been yet undertaken, we decided to investigate the cytotoxicity of the diamines obtained by the acid catalyzed reaction of furfural with dibenzylamine.

Table 1

Compound	**IC_{50} (μM)**
1	3.3 ± 1.0
2	12.0 ± 4.7
3	4.3 ± 0.9
4	41.7 ± 0.7
5	> 100
6	> 100
7	> 100
8	11.1 ± 2.2
9	10.8 ± 1.9
10	69.1 ± 4.7

Table 1: *Citotoxicity determination of the compounds after 48h expeosure to HeLa cell line, IC_{50} values are reported.*

This series of preliminary tests revealed that *N,N,N',N'*-tetrabenzyl-4,5-diamino-2-cyclopentenone (**1**) was cytotoxic in the μM range.

Figure 1

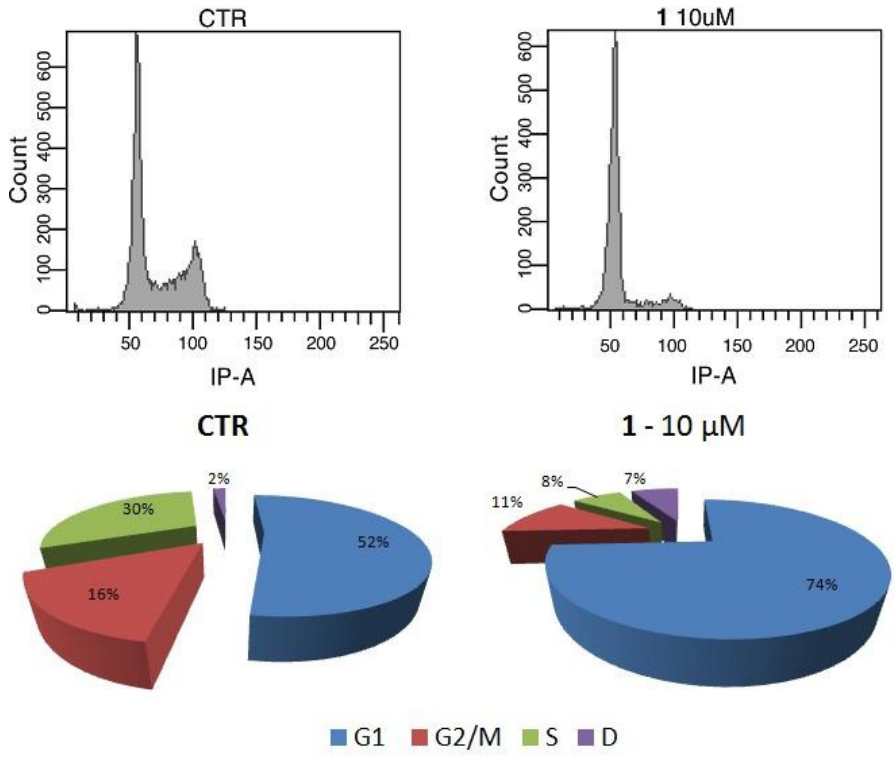

Figure 1: *Cell cycle analysis after 16 hours treatment of HeLa cells with **1** at 10 µM. Pie-charts for the percentages of the different cell phases for control and after treatment with **1** at 10 µM.*

Figure 2

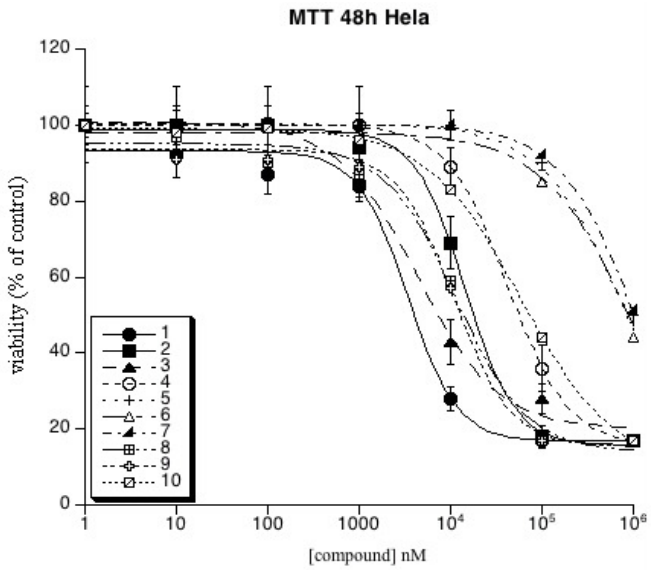

Figure 2: *Dose/response curves for compounds **1**-**10**.*

Figure 3

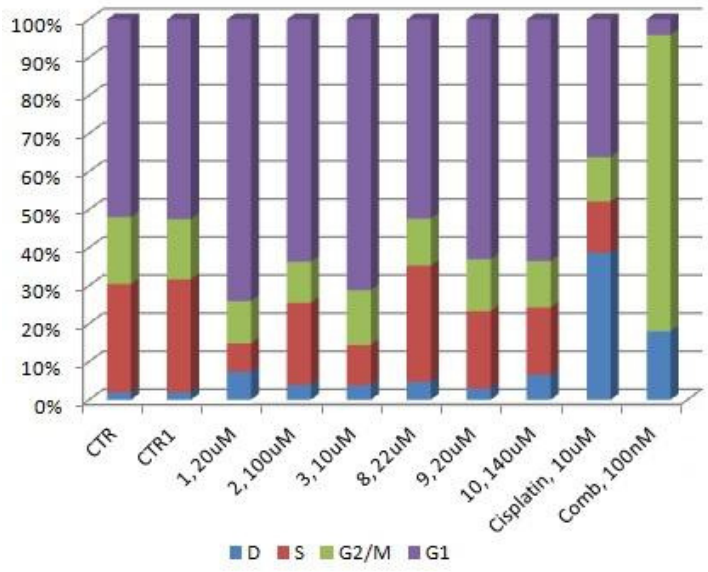

Figure 3: *Histogram representation of cell phases ratios for control and after treatment with **1**, **2**, **3**, **8**, **9**, **10**, cisplatin and combrestatine at the reported concentrations.*

It is interesting to note that compound **1** satisfies all but one Lipinski's Rules (30): there are less than 5 H-bond donors, the molecular weight is less than 500 (MW = 472.6) and there are less than 10 H-bond acceptors (two nitrogen atoms and one ketone). The logP of **1** is the only exception, being higher than 5 (logP = 7.05) as a result of the presence of four aromatic rings; nevertheless one violation of those rules is usually accepted (31). Compound **1** applies as a prototypal lead-compound for drug discovery studies.

Scheme 1

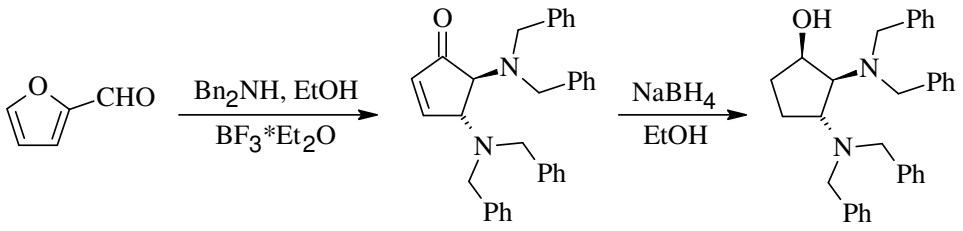

1 **2**

Scheme 1: *Synthesis of N,N,N',N'-tetrabenzyl-4,5-diaminocyclopentenone (**1**) and its reduction to N,N,N',N'-tetrabenzyl-2,3-diaminocyclopentanol (**2**).*

Scheme 2

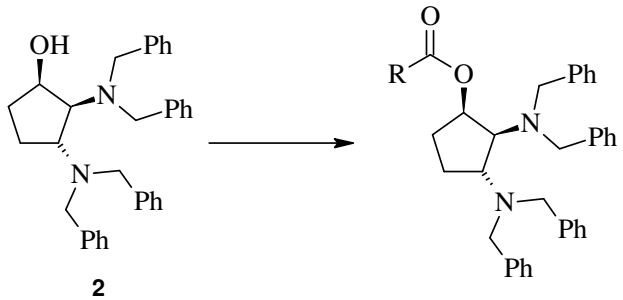

2

R=CH_3 (**3**), C_6H_5 (**4**),
4-NO_2-C_6H_4 (**5**), 4-F-C_6H_4 (**6**),
n-$C_{13}H_{27}$ (**7**)

Scheme 2: *Synthesis of acetyl-, benzoyl-, 4-nitrobenzoyl-, 4-fluorobenzoyl- and hexadecanoyl-derivatives (**3-4-5-6-7**).*

Scheme 3

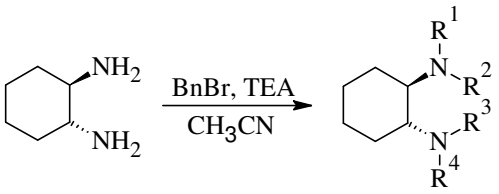

$R^1=R^2=R^3=R^4=$Bn (**8**)
$R^1=R^2=R^3=$Bn $R^4=$H (**9**)
$R^1=R^3=$Bn $R^2=R^4=$H (**10**)

Scheme 3: *Synthesis of tetrabenzylic-, tribenzylic- and N,N'-dibenzylic-derivatives (**8-10**).*

Results and Discussion

Compound **1** was synthesized in racemic form in good yields from the condensation of furfural with dibenzylamine in ethanol; the reaction was catalyzed by BF_3 and run in the presence of 4 Å molecular sieves. Cytotoxicity in HeLa cancer cell line was used as first screening for the bioactivity of this molecule. Dose/response curves were performed exposing cells for 48 hours to concentration of **1** ranging from 10 nM to 100 μM. Gratifyingly the IC_{50} of compound **1** was localized in the micromolar range (3.3 ± 1.0 μM). To further investigate the effect of this molecule we performed a cell cycle analysis after 16 hours of exposure to the drug at different concentrations above the IC_{50} value. Compound **1** showed a clear G1 phase arrest at the concentration of 10μM, clearly recognizable in figure 1. Several antitumoral drugs act blocking cells in G1 phase ultimately leading to cell death, although this can be accomplished by different mechanisms. For example etoposide (32) and irinotecan (33) stop the synthesis of DNA by the inhibition of Topoisomerase. A new class of drugs acts as CDK modulators producing G1 phase arrest, too;

examples for this action are alvocidib (34), P276-00 (35), SNS-032 (36), and roscovitine (37).

The bioactivity of **1** prompted us to carry out a preliminary SAR by preparing selected derivatives (Scheme 1) and screening their cytotoxicity. Reduction of the conjugated ketone with $NaBH_4$ in ethanol afforded the cyclopentanol ring of **2** with complete diastereoselectivity (*cis,trans*- isomer obtained) due to the directing influence of the steric hindrance of the 5-dibenzylamino substituent. *O*-Acetylation and *O*-benzoylation with the corresponding anhydrides in basic condition afforded derivatives **3-4**; 4-nitrobenzoyl-, 4-fluorobenzoyl- and hexadecanoyl-esters were obtained by reaction with the corresponding acyl chloride (compounds **5-7**) in the presence of a suitable base.

As with compound **1**, cytotoxicity in HeLa cancer cell line was used to preliminarily evaluate the bioactivity of the derivatives. Dose/response curves were performed for all compounds on cells treated for 48 h to concentration ranging from 10 nM to 100 μM (figure 2). The resulting IC_{50} values are reported in table 1, showing a hierarchical potency of the compounds as **1~3>2>4>5~6~7.** Cell cycle analysis for compounds **2**-**3** was performed by 16 hours exposure at different concentrations above the IC_{50} specific values for each compound. Only compound **3** showed a clear G1/S transition block at the concentration of 10 μM similar to that observed for compound **1** (figure 3). The percentage of cells in G1 increases about 20% and cells in S phase decrease from 30% to 10%. Compound **2** showed only a weak effect on cell phases ratio at 100 μM, indicating a low efficiency on the cell phase regulation. Compounds **5**-**7** were not examined due to their critically high IC_{50} values. The H-bond acceptor ability of the oxygen atom of compound **1** appears to be important for the activity. Either the reduction of the α,β-unsaturated ketone or the increased steric hindrance, resulting by the acylation of the hydroxyl group to both aromatic and aliphatic esters, reduce the cytotoxic activity of the molecules, as

reported in Table 1. Only the acetylation of the hydroxylic function raised the activity of compound **2** to a level comparable to **1**. The Michael acceptor ability of the α,β-unsaturated ketone of the cyclopentenone ring, known to determine a cytotoxic inhibition of the G_1-CDK activity for prostaglandines PGA_1 and PGA_2 (38, 39), does not appear to play a key role in the activity of these compounds.

Additional work was dedicated to verify if the four benzyl groups present in **1** are involved in the bioactivity. To this purpose, we selected the commercial available *trans*-1,2-cyclohexanediamine to mimic the cyclic backbone of **1** and implanted on the nitrogen atoms a variable number of benzyl groups (n = 2-4) through a standard alkylation procedure; chromatographic separation of the reaction mixture yielded compounds **8**-**10** (Scheme 1).

Cytotoxicity in HeLa cancer cell line for these molecule was evaluated with the same protocol used for compounds **1**-**7**, affording the IC_{50} values for compounds **8**-**10**, reported in table 1. The diamine **8**, bearing four benzyl groups on the two nitrogen atoms of the *trans*-cyclohexanediamine, is structurally the most similar to compounds of the series **1**-**7**. Size and conformational differences between the alicyclic rings were not considered at this preliminary level of screening. The IC_{50} value for this compound is close to that observed for compound **2**, with the lack of the H-bond acceptor group on the cyclohexane ring as a possible reason of the low cytotoxicity. Cytotoxicity is maintained leaving three benzylic substituents, the IC_{50} value of compound **9** being practically the same to that observed for compound **8**. The cytotoxicity dramatically drops when another benzyl group is removed, clearly showing an active role of three benzyl moieties in the mechanism underlying the biological activity.

Cell cycle analysis of these compounds showed no visible effect of **8** on cell cycle ratios, underlining the importance of the H-bond acceptor. A weak effect

at 20 μM was noted for **9**, while the G_1 phase arrest decreases dramatically when the molecule bears only two benzyl groups, showing just a weak effect at 140 μM for compound **10**. If the removal of one benzyl has practically no effect on the IC_{50} value, the block of the G_1/S transition seems to be influenced, likely suggesting the overall polarity of the molecule as additional parameter involved.

Conclusions

Interesting bioactivities were observed in *N*-benzylated alicyclic 1,2-diamines. The most actives compounds, **1** and **3**, showed IC_{50} values of 3.3 and 4.3 μM respectively on HeLa cancer cells. Analysis of the cell cycle showed selective blocking of the G_1/S transition (G_1 phase arrest). Preliminary SAR studies evidenced the importance of a H-bond acceptor close to the amine groups and at least 3 benzyl groups on the nitrogen atoms to retain the reported activity. A pharmacological study will be undertaken in order to identify the biological target(s) linked to the G_1/S transition block underlying the cytotoxicity of these compounds. A wider SAR will be useful to explore in detail this class of molecules and to identify original compounds with improved cytotoxicity profiles.

Experimental

***N,N,N',N'*-Tetrabenzyl- 4,5-diamino-2-cyclopenten-1-one (1)**

Furfural (20.0 g, 208 mmol) and dibenzylamine (82.1 g, 416 mmol) were dissolved in ethanol (150 mL). Boron trifluoride etherate (14.8 g, 104 mmol) and 4Å molecular sieves were added and the resulting reaction mixture was stirred at room temperature for 2 days. The reaction mixture is then heated to reflux and filtered hot. On cooling the filtrate released a voluminous precipitate, isolated by centrifugation and washed with cold ethanol. The product was dried in vacuum, affording *N*,*N*,*N'*,*N'*-tetrabenzyl- 4,5-diamino-2-cyclopenten-1-one **1** (81.6 g, 83%) as a yellowish powder. ^{1}H-NMR ($CDCl_3$, 300MHz, 298K) δ: 7.58 (dd, 1H, J=6.1, 2.1Hz), 7.36-7.19 (m, 20H), 6.20 (dd, 1H, J=6.1, 1.8Hz), 4.06 (dt, 1H, J_d=2.8Hz, J_t=2.1Hz), 3.83 (d, 2H, J=13.2Hz), 3.62 (d, 1H, J=3.1Hz), 3.55 (d, 2H, J=13.2Hz), 3.39 (s, 4H). ^{13}C-NMR ($CDCl_3$, 75.4MHz, 298K) δ: 206.1 (C), 163.1 (CH), 139.4 (C), 135.6 (CH), 129.6 (CH), 128.7 (CH), 128.35 (CH), 128.29 (CH), 127.24 (CH), 127.17 (CH), 64.5 (CH), 63.4 (CH), 55.1 (CH_2), 54.7 (CH_2). Mp=106-107 °C.

***N,N,N',N'*-Tetrabenzyl-2,3-diaminocyclopentan-1-ol (2)**

N,*N*,*N'*,*N'*-tetrabenzyl-4,5-diamino-2-cyclopenten-1-one **1** (20.0 g, 42.4 mmol) was dissolved in 2-propanol (250 mL) and sodium borohydride (6.4 g, 169.6 mmol) was added at room temperature. The resulting reaction mixture was stirred at room temperature for 3 hours, checking periodically by TLC (CH_2Cl_2/MeOH 9/1). The solution was cooled to 0°C with an ice bath and 200 mL of 2M HCl solution was slowly added with vigorous stirring. After 30 minutes, sodium carbonate was added in small portions to bring to pH 10 and the resulting aqueous solution was extracted thrice with dichloromethane. The

organic extracts were combined and dried over sodium sulfate. The drying agent was filtered and washed with dichloromethane. The solvent was removed by evaporation under reduced pressure, affording *N*,*N*,*N'*,*N'*-tetrabenzyl-2,3-diaminocyclopentan-1-ol (19.8 g, 98%) as a white solid. ^{1}H-NMR ($CDCl_3$, 300MHz, 298K) δ: 7.41-7.16 (m, 20H), 3.98 (q, 1H, J=4.8Hz), 3.89 (d, 2H, J=14.4Hz), 3.82 (d, 2H, J=13.5Hz), 3.74-3.62 (m, 1H), 3.61 (d, 2H, J=14.1Hz), 3.36 (d, 2H, J=13.5Hz), 3.28 (dd, 1H, J=8.4, 6.0Hz), 2.07-1.81 (m, 2H), 1.80-1.64 (m, 2H). ^{13}C-NMR ($CDCl_3$, 75.4MHz, 298K) δ: 139.56 (C), 139.46 (C), 129.3 (CH), 128.9 (CH), 128.4 (CH), 127.2 (CH), 127.0 (CH), 70.8 (CH), 65.4 (CH), 60.7 (CH), 55.8 (CH_2), 55.0 (CH_2), 31.5 (CH_2), 19.0 (CH_2).

***N,N,N',N'*-tetrabenzyl-2,3-diaminocyclopent-1-yl acetate (3)**

N,*N*,*N'*,*N'*-Tetrabenzyl-2,3-diaminocyclo-pentan-1-ol **2** (250 mg, 0.525 mmol) was dissolved in dichloromethane (5 mL). Acetic anhydride (100 µL, 107 mg, 1.05 mmol) and 4-dimethylaminopyridine (13 mg, 0.10 mmol) were added at room temperature and the resulting reaction mixture was stirred overnight. The solution was washed thrice with a saturated solution of sodium carbonate and twice with a saturated solution of sodium chloride. The organic phase was then dried over sodium sulfate, filtered and the solvent was removed by evaporation under reduced pressure. The crude product was purified by gravimetric chromatography on silica gel column (petroleum ether/ethyl acetate 95:5 as eluant) giving 250 mg of *N*,*N*,*N'*,*N'*-tetrabenzyl-2,3-diaminocyclopent-1-yl acetate (248 mg, 0.49 mmol, 93%) as a white amorphous solid. ^{1}H-NMR ($CDCl_3$, 300MHz, 298K) δ: 7.54-7.24 (m, 20H), 5.42 (td, 1H, J_t=5.3Hz, J_d=2.2Hz), 3.96 (d, 2H, J=14.4Hz), 3.91-3.79 (m, 1H), 3.87 (d, 2H, J=13.8Hz), 3.74 (d, 2H, J=14.4Hz), 3.42 (d, 2H, J=13.5Hz), 3.35 (dd, 1H, J=10.4, 5.5Hz), 2.03 (s, 3H), 1.99-1.83 (m, 2H), 1.73-1.58 (m, 2H). ^{13}C-NMR ($CDCl_3$, 75.4MHz, 298K) δ: 170.8 (C), 140.7 (C), 140.0 (C), 129.1 (CH), 128.5 (CH),

128.4 (CH), 127.1 (CH), 126.9 (CH), 75.3 (CH), 61.8 (CH), 58.7 (CH), 55.6 (CH_2), 54.4 (CH_2), 28.8 (CH_2), 21.8 (CH_3), 18.7 (CH_2).

***N,N,N',N'*-tetrabenzyl-2,3-diaminocyclopent-1-yl Benzoate (4)**

N,*N*,*N'*,*N'*-Tetrabenzyl-2,3-diaminocyclo-pentan-1-ol **2** (250 mg, 0.525 mmol) was dissolved in dichloromethane (5 mL). Benzoic anhydride (240 mg, 1.05 mmol) and 4-dimethylaminopyridine (13 mg, 0.1 mmol) were added at room temperature and the resulting reaction mixture was stirred overnight. The solution was washed thrice with a saturated solution of sodium carbonate and twice with a saturated solution of sodium chloride. The organic phase was then dried over sodium sulfate, filtered and the solvent was removed by evaporation under reduced pressure. The crude product was purified by gravimetric chromatography on silica gel column (petroleum ether/ethyl acetate 95:5 as eluant) affording *N*,*N*,*N'*,*N'*-tetrabenzyl-2,3-diaminocyclopent-1-yl benzoate (170 mg, 56%) as a white solid. ^{1}H-NMR ($CDCl_3$, 300MHz, 298K) δ: 7.94 (d, 2H, J=8.3Hz), 7.63-7.19 (m, 23H), 5.68 (bs, 1H), 3.99 (d, 2H, J=13.8Hz), 3.98-3.82 (m, 1H), 3.88 (d, 2H, J=13.4Hz), 3.67 (d, 2H, J=14.1Hz), 3.42 (d, 2H, J=13.5Hz), 3.43-3.34 (m, 1H), 2.05-1.86 (m, 2H), 1.84-1.63 (m, 2H). ^{13}C-NMR ($CDCl_3$, 75.4MHz, 298K) δ: 166.1 (C), 140.5 (C), 140.0 (C), 133.0 (CH), 130.8 (C), 129.8 (CH), 129.2 (CH), 128.6 (CH), 128.5 (CH), 128.33 (CH), 128.28 (CH), 127.0 (CH), 126.9 (CH), 74.9 (CH), 62.0 (CH), 58.2 (CH), 55.3 (CH_2), 54.4 (CH_2), 28.5 (CH_2), 18.1 (CH_2).

***N,N,N',N'*-Tetrabenzyl-2,3-diaminocyclopent-1-yl 4-Nitrobenzoate (5)**

N,*N*,*N'*,*N'*-Tetrabenzyl-2,3-diaminocyclopentan-1-ol **2** (250 mg, 0.525 mmol) was dissolved in dichloromethane (5 mL). 4-Nitrobenzoyl chloride (195 mg, 1.05 mmol), triethylamine (290 µL, 160 mg, 2.1 mmol) and 13 mg of 4-dimethylaminopyridine (13 mg, 0.1 mmol) were added at room temperature and

the resulting reaction mixture was stirred for 3 hours, checking periodically by TLC. The solution was washed thrice with a saturated solution of sodium carbonate and twice with a saturated solution of sodium chloride. The organic phase was then dried over sodium sulfate, filtered and the solvent was removed by evaporation under reduced pressure. The crude product was purified by gravimetric chromatography on silica gel column (petroleum ether/ethyl acetate 95:5 as eluant) giving *N*,*N*,*N'*,*N'*-tetrabenzyl-2,3-diaminocyclopent-1-yl 4-nitrobenzoate (290 mg, 0.46 mmol, 88%) as a white solid. ^{1}H-NMR ($CDCl_3$, 300MHz, 298K) δ: 8.20 (d, 2H, J=8.6Hz), 7.97 (d, 2H, J=8.6Hz), 7.55-7.14 (m, 20H), 5.62 (bs, 1H), 3.92 (d, 2H, J=14.7Hz), 3.88 (d, 2H, J=14.1Hz), 3.97-3.81 (m, 1H), 3.61 (d, 2H, J=14.1Hz), 3.45-3.32 (m, 1H), 3.38 (d, 2H, J=13.2Hz), 2.09-1.83 (m, 2H), 1.81-1.63 (m, 2H). ^{13}C-NMR ($CDCl_3$, 75.4MHz, 298K) δ: 164.2 (C), 150.5 (C), 140.2 (C), 139.7 (C), 136.0 (C), 130.7 (CH), 129.2 (CH), 128.3 (CH), 127.1 (CH), 126.9 (CH), 123.6 (CH), 76.4 (CH), 62.0 (CH), 58.1 (CH), 55.5 (CH_2), 54.4 (CH_2), 28.3 (CH_2), 17.7 (CH_2).

***N,N,N',N'*-Tetrabenzyl-2,3-diaminocyclopent-1-yl 4-Fluorobenzoate (6)**

N,*N*,*N'*,*N'*-Tetrabenzyl-2,3-diaminocyclopentan-1-ol **2** (250 mg, 0.525 mmol) was dissolved in dichloromethane (5 mL). 4-Fluorobenzoyl chloride (165 mg, 1.05 mmol), triethylamine (290 µL, 160 mg, 2.1 mmol) and 4-dimethylaminopyridine (13 mg, 0.1 mmol) were added at room temperature and the resulting reaction mixture was stirred for 18 hours, checking periodically by TLC. The solution was washed thrice with a saturated solution of sodium carbonate and twice with a saturated solution of sodium chloride. The organic phase was then dried over sodium sulfate, filtered and the solvent was removed by evaporation under reduced pressure. The crude product was purified by gravimetric chromatography on silica gel column (petroleum ether/ethyl acetate 95:5 as eluant) affording *N*,*N*,*N'*,*N'*-tetrabenzyl-2,3-diaminocyclopent-1-yl 4-

fluorobenzoate (190 mg, 61%) as a white solid. ^{1}H-NMR ($CDCl_3$, 300MHz, 298K) δ: 8.27-8.18 (m, 2H), 7.98-7.89 (m, 2H), 7.60-7.19 (m, 18H), 7.11 (t, 2H, J=8.7Hz), 5.75-5.63 (m, 1H), 4.04-3.86 (m, 1H), 3.99 (d, 2H, J=14.1Hz), 3.90 (d, 2H, J=13.1Hz), 3.67 (d, 2H, J=14.1Hz), 3.43 (d, 2H, J=13.4Hz), 3.49-3.35 (m, 1H), 2.07-1.87 (m, 2H), 1.83-1.66 (m, 2H). ^{13}C-NMR ($CDCl_3$, 75.4MHz, 298K) δ: 168.6 (C), 167.5 (C), 162.8 (d, C, J_{CF}=211.8Hz), 140.4 (C), 139.9 (C), 133.4 (d, CH, J_{CF}=9.8Hz), 129.2 (CH), 128.6 (CH), 128.4 (CH), 128.3 (CH), 127.1 (CH), 126.9 (CH), 116.4 (d, CH, J_{CF}=21.9Hz), 75.2 (CH), 62.0 (CH), 58.2 (CH), 55.4 (CH_2), 54.4 (CH_2), 28.4 (CH_2), 18.0 (CH_2).

***N,N,N',N'*-Tetrabenzyl-2,3-diaminocyclopent-1-yl Palmitate** (**7**)

N,*N*,*N'*,*N'*-Tetrabenzyl-2,3-diaminocyclo-pentan-1-ol **2** (250 mg, 0.525 mmol) was dissolved in dichloromethane (5 mL). Palmitoyl chloride (260 mg, 1.05 mmol), triethylamine (290 µL, 160 mg, 2.1 mmol) and 4-dimethylaminopyridine (13 mg, 0.1 mmol, 0.2 eq) were added at room temperature and the resulting reaction mixture was stirred for 3 hours, checking periodically by TLC. The solution was washed thrice with a saturated solution of sodium carbonate and twice with a saturated solution of sodium chloride. The organic phase was then dried over sodium sulfate, filtered and the solvent was removed by evaporation under reduced pressure. The crude product was purified by gravimetric chromatography on silica gel column (petroleum ether/ethyl acetate 98:2 as eluant) affording *N*,*N*,*N'*,*N'*-tetrabenzyl-2,3-diaminocyclopent-1-yl palmitate (150 mg, 40%) as a white solid. ^{1}H-NMR ($CDCl_3$, 300MHz, 298K) δ: 7.42-7.18 (m, 20H), 5.39-5.29 (m, 1H), 3.87 (d, 2H, J=14.1Hz), 3.78 (d, 2H, J=13.5Hz), 3.82-3.72 (m, 1H), 3.62 (d, 2H, J=14.1Hz), 3.39 (d, 2H, J=13.7Hz), 3.33-3.23 (m, 1H), 2.24-2.16 (m, 2H), 1.92-1.77 (m, 2H), 1.71-1.47 (m, 4H), 1.40-1.18 (m, 24H), 0.89 (t, 3H, J=6.7Hz).

_N_-Benzylated trans-1,2-Diaminocyclohexanes (8-10)

trans-1,2-Diaminocyclohexane (1.0 g, 8.8 mmol) was dissolved in acetonitrile (10 mL). Benzyl bromide (6.0 g, 35 mmol) was added dropwise and the resulting solution was stirred at room temperature for 15 minutes. Triethylamine (4.4 g, 43.8 mmol) was added dropwise during a period of 15 minutes and the resulting reaction mixture was stirred at room temperature overnight. The solvent was removed by evaporation under reduced pressure; the residue was paritioned thrice between diethyl ether and 2M HCl. The aqueous extracts were combined and sodium carbonate was carefully added until pH 9. The resulting solution was extracted thrice with dichloromethane. The organic extracts were combined, dried over sodium sulfate, filtered and the solvent was removed by evaporation under reduced pressure. The resulting mixture was separated by gravimetric chromatography on silica gel column (petroleum ether/ethyl acetate, 9:1→7:3 gradient), obtaining *N*,*N*,*N'*,*N'*-tetrabenzyl-*trans*-1,2-diaminocyclohexane (3.08 g, 74%), *N*,*N*,*N'*-tribenzyl-*trans*-1,2-diaminocyclohexane (130 mg, 4%) and *N*,*N'*-dibenzyl-*trans*-1,2-diaminocyclohexane (330 mg, 13%).

***N,N,N',N'*-tetrabenzyl-trans-1,2-diaminocyclohexane**

^{1}H-NMR ($CDCl_3$, 300 MHz, 298K) δ: 7.47-7.40 (m, 8H), 7.31-7.19 (m, 12H), 3.79 (d, 4H, J=13.8Hz), 3.37 (d, 4H, J=13.8Hz), 2.78-2.66 (m, 2H), 2.18-2.03 (m, 2H), 1.78-1.65 (m, 2H), 1.20-0.99 (m, 4H). ^{13}C-NMR ($CDCl_3$, 75.4 MHz, 298K) δ: 140.7 (C), 129.0 (CH), 128.1 (CH), 126.7 (CH), 58.3 (CH), 53.4 (CH_2), 26.1 (CH_2), 25.1 (CH_2).

***N,N,N'*-tribenzyl-trans-1,2-diaminocyclohexane**

^{1}H-NMR ($CDCl_3$, 300 MHz, 298K) δ: 7.42-7.18 (m, 15H), 3.87 (d, 2H, J=13.2Hz), 3.76 (d, 4H, J=13.8Hz), 3.55 (d, 2H, J=13.2Hz), 3.42 (d, 4H, J=13.8Hz), 2.96 (bs, 1H, exchange with D_2O), 2.64-2.46 (m, 2H), 2.14 (d, 1H, J=12.6Hz), 2.02 (d, 1H, J=12.3Hz), 1.90-1.61 (m, 2H), 1.42-0.95 (m, 4H). ^{13}C-NMR ($CDCl_3$, 75.4 MHz, 298K) δ: 141.1 (C), 140.1 (C), 128.8 (CH), 128.43 (CH), 128.38 (CH), 128.28 (CH), 127.0 (CH), 126.8 (CH), 62.2 (CH), 58.0 (CH), 53.9 (CH_2), 51.7 (CH_2), 32.0 (CH_2), 25.8 (CH_2), 24.8 (CH_2), 22.8 (CH_2).

***N,N'*-dibenzyl-trans-1,2-diaminocyclohexane**

^{1}H-NMR ($CDCl_3$, 300 MHz, 298K) δ: 7.38-7.15 (m, 10H), 3.95 (d, 2H, J=13.5Hz), 3.49 (s, 2H, exchange with D_2O), 3.34 (d, 2H, J=13.2Hz), 2.40-2.26 (m, 2H), 2.02-1.70 (m, 4H), 1.40-1.17 (m, 4H). ^{13}C-NMR ($CDCl_3$, 75.4 MHz, 298K) δ: 135.4 (C), 128.6 (CH), 128.3 (CH), 126.9 (CH), 69.4 (CH), 58.1 (CH_2), 29.8 (CH_2), 24.5 (CH_2).

References

1 Ferlay J, Shin H-R, Bray F, Forman D, Mathers C, Maxwell Parkin D (2010), Estimates of worldwide burden of cancer in 2008: GLOBOCAN 2008. *Int. J. Cancer*, **127**, 2893-2917.

2 Jemal A, Bray F, Center M M, Ferlay J, Ward E, Forman D (2011), Global cancer statistics. *CA Cancer J. Clin.*, **61**, 69-90.

3 Lucet D, Le Gall T, Mioskowski C (1998), The chemistry of vicinal diamines. *Ang. Chem. Int. Ed. Engl.*, **37**, 2580-2647.

4 Michalson E T, Szmuszkovicz J (1989), Medicinal agents incorporating the 1,2-diamine functionality. *Prog. Drug. Res.*, **33**, 135-149.

5 Szmuszkovicz J, VonVoigtlander P F, Kane M P (1981), A new nontricyclic antidepressant agent. Synthesis and activity of *N*-[trans-2-(dimethy1amino)cyclopenty1]-*N*-(3,4-dichlorophenyl)propanamide and related compounds. *J. Med. Chem.*, **24**, 1230-1236.

6 Zubovics Z, Toldy L, Varrò A, Rabloczky G, Kürthy M, Dvortsàk P, Jerkovich G, Tomori E (1986), Synthesis and antiarrhythmic activity of *N*-arylalkylenediamines. *Eur. J. Med. Chem.*, **21**, 370-378.

7 Musa M A, Khan M O, Aspedon A, Cooperwood J S (2010), Synthesis and antimicrobial activity of *N,N′*-bis(2-hydroxylbenzyl)-1,2-ethanediamine derivatives. *Lett. Drug. Des. Discov.*, **7**, 165-170.

8 Leal S M, Amado D F, Kouznetsov V V, Escobar P (2013), In vitro antileishmanial, trypanocidal, and mammalian cell activities of diverse *N,N′*-dihetaryl substituted diamines and related compounds. *Sci. Pharm.*, **81**, 43-55.

9 Rebollo O, Del Olmo E, Ruiz G, López-Pérez J L, Giménez A, San Feliciano A (2008), Leishmanicidal and trypanocidal activities of 2-aminocyclohexanol

and 1,2-cyclohexanediamine derivatives. *Bioorg. Med. Chem. Lett.*, **18**, 184-187.

10 Rosenberg B, VanCamp L, Trosko JE, Mansour VH (1969), Platinum compounds: a new class of potent antitumour agents. *Nature*, **222**, 385-386.

11 Reedijk J (1996), Improved understanding in platinium antitumour chemistry. *Chem. Commun.*, 801-806.

12 Gust R, Burgemeister T, Mannschreck A, Schoenenberger H (1990), Aqua[1-(2,6-dichloro-4-hydroxyphenyl)-2-phenylethylenediamine](sulfato)platinum-(II) complexes with variable substituents in the 2-phenyl ring. 1. Synthesis and antitumor and estrogenic properties. *J. Med. Chem.*, **33**, 2535-2544.

13 Kelland L R, Abel G, McKeage M J, Jones M, Goddard P M, Valenti M, Murrer B A, Harrap K R (1993), Preclinical antitumor evaluation of bis-acetato-ammine-dichloro-cyclohexylamine platinum(IV): an orally active platinum drug. *Cancer Res.*, **53**, 2581-2586.

14 Brunner H, Hankofer P, Holzinger U, Treittinger B, Schönenberger H (1990), Synthesis and antitumor activity of platinum(II) complexes containing substituted ethylenediamine ligands. *Eur. J. Med. Chem.*, **25**, 35-44.

15 Brunner H, Hankoferm P, Holzinger U, Treittinger B (1990), Synthesis and antitumor activity of Pt(II) complexes of benzyl-1,2-diaminoethane ligands. *Chem. Ber.*, **123**, 1029-1038.

16 Kim D-K, Kim Y-W, Kim H-T, Kim KH (1996), Synthesis and *in vitro* cytotoxicity of *cis*-dichloro[(2*S*,3*R*,4*S*)-2-aminomethyl-3,4-(*O*-isopropylidene)dihydroxy- or -3,4-dihydroxypyrrolidine]platinum(II). *Bioorg. Med. Chem. Lett.*, **6**, 643-646.

17 Khokhar A R, Al-Baker S, Shamsuddin S, Siddik Z H (1997), Chemical and biological studies on a series of novel (trans-(1R,2R)-, trans-(1S,2S)-, and cis-

1,2-diaminocyclohexane)platinum(IV) carboxylate complexes. *J. Med. Chem.*, **40**, 112-116.

18 McRipley R J, Burns-Horwitz P E, Czerniak P M, Diamond R J, Diamond M A, Miller J L D, Page R J, Dexter D L, Chen S-F, Sun J-H, Behrens C H, Seitz S P, Gross J L (1994), Efficacy of DMP 840: a novel bis-naphthalimide cytotoxic agent with human solid tumor xenograft selectivity. *Cancer Research*, **54**, 159-164.

19 Cherney R J, Swartz S G, Patten A D, Akamike E, Sun J-H, Kaltenbach III R F, Seitz S P, Behrens C H, Getahun Z, Trainor G L, Vavala M, Kirshenbaum M R, Papp L M, Stafford M P, Czerniak P M, Diamond R J, McRipley R J, Page R J, Gross J L (1997), The synthesis and antitumor evaluation of unsymmetrical bis-imides. *Bioorg. Med. Chem. Lett.*, **7**, 163-168.

20 Kulanthaivel P, Hallock Y F, Boros C, Hamilton S M, Janzen W P, Ballas L M, Loomis C R, Jiang J B, Katz B (1993), Balanol: a novel and potent inbibitor of protein kinase C from the fungus *Verticillium balanoides*. *J. Am. Chem. Soc.*, **115**, 6452-6453.

21 Hoffmann T (1998), Characterization f the chemical structure of novel colored Maillard reaction products from furan-2-carboxaldehyde and amino acids. *J. Agric. Food. Chem.*, **46**, 932-940.

22 Li S-W, Batey R A (2007), Mild lanthanide(III) catalyzed formation of 4,5-diaminocyclopent-2-enones from 2-furaldehyde and secondary amines: a domino condensation/ring-opening/electrocyclization process. *Chem. Commun.*, **36**, 3759-3761.

23 Prokhorov A, Le Bris N, Bernard H, Claudon G, Handel H (2006), Cyclohexanedione bisaminals as intermediates for cyclen, homocyclen, and cyclam synthesis. *Synth. Comm.*, **36**, 3271-3282.

24 Nicholson E S, Ashworth B T (1977), *US Pat.,* 4013720.

25 Lewis K J, Mulquiney C E (1977), Aspects of the formation and use of Stenhouse salts and related compounds. *Tetrahedron*, **33**, 463-475.

26 Stenhouse J (1850), Ueber die oele, die bei der einwirkung der schwefelsäure auf verschiedene vegetabilien entstehen. *J. Liebigs Ann. Chem.*, **74**, 278-297.

27 McGowan J C (1949), The preparation of bases from the coloured compounds formed by condensation of furfuraldehyde with aromatic amines. *J. Chem. Soc.*, **165**, 777-779.

28 Stenhouse J (1870), Ueber Furfuranilin und Furfurtoluidin. *Ann.*, **156**, 197-205.

29 Dieckmann D, Beck B (1905), Ueber Farbstoffe aus Furfurol. *Ber.*, **38**, 4122-4125.

30 Lipinski C A, Lombardo F, Dominy B W, Feeney P J (1997), Experimental and computational approaches to estimate solubility and permeability in drug discovery and development settings. *Adv. Drug Deliv. Rev.*, **23**, 3-25.

31 Keller T H, Pichota H, Yin Z (2006), A practical view of 'druggability'. *Curr. Op. Chem. Biol.*, **10**, 357-361.

32 Minocha A, Long B H (1984), Inhibition of the DNA catenation activity of type II topoisomerase by VP16-213 and VM26. *Biochem. Biophys. Res. Commun.*, **122**, 165-170.

33 Tsuruo T, Matsuzaki T, Matsushita M, Saito H, Yokokura T (1988), Antitumor effect of CPT-11, a new derivative of camptothecin, against pleiotropic drug-resistant tumors in vitro and in vivo. Cancer *Chemother. Pharmacol.*, **21**, 71-74.

34 Drees M, Dengler W A, Roth T, Labonte H, Mayo J, Malspeis L, Grever M, Sausville E A, Fiebig H H (1997), Flavopiridol (L86-8275): selective antitumor activity in vitro and activity in vivo for prostate carcinoma cells. Clin. *Cancer Res.*, **3**, 273-279.

35 Raje N, Hideshima T, Mukherjee S, Raab M, Vallet S, Chetri S, Cirstea D, Pozzi S, Mitsiades C, Rooney M, Kiziltepe T, Podar K, Okawa Y, Ikeda H, Carrasco R, Richardson P G, Chauhan D, Munshi N C, Sharma S, Parikh H, Chabner B, Scadden D, Anderson K C (2009), Preclinical activity of P276-00, a novel small-molecule cyclin-dependent kinase inhibitor in the therapy of multiple myeloma. *Leukemia*, **23**, 961-970.

36 Heath E I, Bible K, Martell R E, Adelman D C, Lorusso P M (2008), A phase 1 study of SNS-032 (formerly BMS-387032), a potent inhibitor of cyclin-dependent kinases 2, 7 and 9 administered as a single oral dose and weekly infusion in patients with metastatic refractory solid tumors. *Invest. New Drugs*, **26**, 59-65.

37 Mgbonyebi O P, Russo J, Russo I H (1998), Roscovitine inhibits the proliferative activity of immortal and neoplastic human breast epithelial cells. *Anticancer Res.*, **18**, 751-755.

38 Ohno K, Sakai T, Fukushima M, Narumiya S, Fujiwara M (1988), Site and mechanism of growth inhibition by prostaglandins. IV. Effect of cyclopentenone prostaglandins on cell cycle progression of G1-enriched HeLa S3 cells. *J. Pharmacol. Exp. Ther.*, **245**, 294-298.

39 Gorospe M, Liu Y, Xu Q, Chrest F J, Holbrook N J (1996), Inhibition of G1 cyclin-dependent kinase activity during growth arrest of human breast carcinoma cells by prostaglandin A2. *Mol. Cell. Biol.*, **16**, 762-770.

Conclusions

The research activity of the PhD project was centered on the design, preparation and preliminary evaluation of components of nanosized systems for Molecular Imaging applications, with a special focus on the development of MRI contrast agents.

During the PhD period, different topics of this wide area of research were examined, three of them reaching full completion and being reported in this thesis.

The first period was devoted to the design, preparation and testing of original amphiphilic Mn-based MRI contrast agents. Three novel EDTA-like chelating agents, bearing one or two long aliphatic chains placed on the ethylenediamine backbone were synthesized and the corresponding Mn(II)-chelates investigated by relaxometric techniques. The latter showed that the amphiphilic chelates easily forms supramolecular aggregates and are therefore useful for the preparation of lipid-based nanosystem such as micelles and liposomes. Moreover and quite surprisingly, the interaction of the amphiphilic complexes with human serum albumin led to the observation of a remarkable increase of the relaxivity, reaching values one order of magnitude higher than those observed with clinically used Gd-based CAs. This work allowed to demonstrate the possibility to use cheaper (and possibly safer) Mn(II)-chelates in place of the currently employed Gd(III)-chelates for this application, and that their efficiency may be comparable with their lanthanide couterpart, provided that suitable conditions (*i.e.*: the inclusion in a nanosized system) are adopted.

The second activity involved the preparation of a unimolecular nanosized chelating agent, prepared by functionalization of polyethyleneimine with phosphonic groups. Complexation of Gd(III) with the polytopic ligand led to a

polynuclear nanosized complex, whose potential as MRI CA was evaluated through extensive relaxometric characterization. The Gd-polyethyleneimine-phosphonate system shows a satisfactory thermodynamic stability, precluding an easy release of toxic Gd(III) ions *in vivo*, and is endowed with a relaxivity value well over 10 $mM^{-1}s^{-1}$. NMRD profiles evidenced the presence of metal ions with a low degree of hydration, largely compensated from a fast coordinated water exchange rate, a likely significant contributions from water molecule in the outer coordination sphere(s) and the slow tumbling rate of the nanometric polymeric molecule. Addition of a cationic surface modifier (meglumine), strongly improved the properties of the nanosized CA: the relaxivity raised due to the increase of the size and the hydration of the coated polymeric nanoparticle, and both solubility and thermodynamic stability of the system were enhanced as a consequence of the shielding effect of the hydrophilic cationic coating.

Finally, during the routine periodical screening of the toxicity of the chelating agents and their synthetic precursor, a biological activity was noticed for a family of diamines used as synthons for the preparation of rigidified ligands for Mn(II). Investigation of this biological activity uncovered an unexpected block in the G1 phase of the cell cycle for some components of this family of diamines. This result shed a light on the importance of screening the toxicity of novel compounds, especially when they are devised for an *in vivo* use.

List of publications

Botta M, De Biasio V, Giovenzana G B, Rolla G, Tei L, "Supramolecular assemblies based on amphiphilic Mn^{2+}-Complexes as High Relaxivity MRI probes", submitting to Chemistry - an Asian Journal

Aime S, Gianolio E, Giovenzana G B, De Biasio V, "Phosphonated polyethyleneimine (PEI-P): evaluation of a chelating polymer as a unimolecular nanosized MRI contrast agents", submitting to RSC Advances

Caldarelli A, De Biasio V, Giovenzana G B, Mastronardo G, Negri R, "*N*-Polybenzylated Alicyclic 1,2-Diamines Show Cytotoxicity and G1 Phase Arrest in Cancer Cell Line", submitted to Molecular Diversity, manuscript number MODI-DI-13-00237R1.

Acknowledgments

The groups of Prof. S. Aime (MBC Center, Università degli Studi di Torino), Prof. M. Botta and Dr. L. Tei (DiSIT, Università degli Studi del Piemonte Orientale) are gratefully acknowledged for their helpful contributions to the relaxometric measurements reported in the present thesis.
The group of Prof. R.N. Muller and in particular Prof. Sophie Laurent (Department of General, Organic and Biomedical Chemistry & Center for Microscopy and Molecular Imaging (CMMI), University of Mons, Belgium) are deeply acknowledged for their kind hospitality in their research structure.
My personal thanks to all lab fellows of these three years, to Cage Chemicals srl, to my family, to Enza, Floraiana, Cip, Riccardo, Livio and all my friends!

VDB